Evolution of Vanadium Redox Flow Battery in Electrode

Md Hasnat Hossain[1], Norulsamani Abdullah[2,3,*], Kim Han Tan[2], R. Saidur[2,3,4,*], Mohd Amran Mohd Radzi[1], Suhaidi Shafie[1]

[1]*Department of Electrical and Electronic Engineering, Universiti Putra Malaysia, 43400 UPM Serdang, Selangor, Malaysia*
[2]*Research Center for Nano-Materials and Energy Technology (RCNMET), School of Engineering and Technology, Sunway University, Bandar Sunway, Petaling Jaya, 47500, Selangor Darul Ehsan, Malaysia*
[3]*Sunway Materials Smart Science & Engineering (SMS2E) Cluster, Sunway University, Petaling Jaya, Selangor, 47500, Malaysia*
[4]*School of Engineering, Lancaster University, Lancaster, LA1 4YW, UK*

Corresponding authors: nabdullah@sunway.edu.my; saidur@sunway.edu.my

ABSTRACT

The vanadium redox flow battery (VRFB) is a highly regarded technology for large-scale energy storage due to its outstanding features, such as scalability, efficiency, long lifespan, and site independence. This paper provides a comprehensive analysis of its performance in carbon-based electrodes, along with a comprehensive review of the system's principles and mechanisms. It discusses potential applications, recent industrial involvement, and economic factors associated with VRFB technology. The study also covers the latest advancements in VRFB electrodes, including electrode surface modification and electrocatalyst materials, and highlights their effects on the VRFB system's performance. Additionally, the potential of two-dimensional material MXene to enhance electrode performance is evaluated, and the author concludes that MXenes offer significant advantages for use in high-power VRFB at a low cost. Finally, the paper reviews the challenges and future development of VRFB technology.

Keywords: Electrode, Electrocatalyst, MXene, Vanadium Redox Flow Battery, Large-Scale Energy Storage.

GRAPHICAL TABLE OF CONTENT

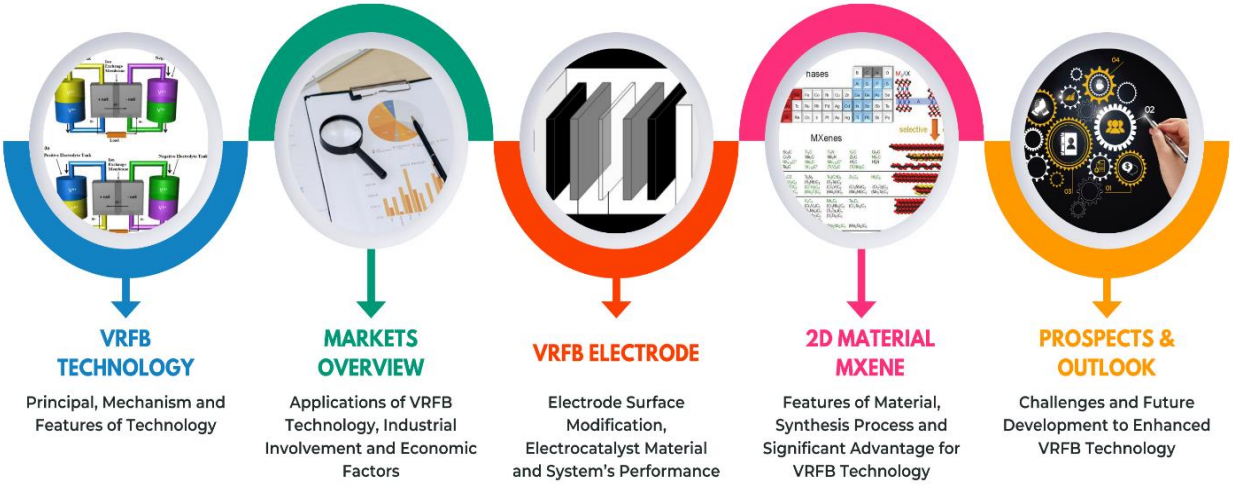

AUTHOR BIOGRAPHIES

Md Hasnat Hossain was born in Khulna, Bangladesh in 1995. He received his B. Eng. (Hons.) in Electrical and Electronic Engineering from Daffodil International University (DIU), in 2019. He is currently doing his M.Sc. degree in Electrical Power Engineering from Universiti Putra Malaysia (UPM). He is also attached with Research Center for Nano-Materials and Energy Technology (RCNMET) in Sunway University. His research interests are renewable energy, redox flow battery, 2D nanomaterials, electrochemical energy storage.

Norulsamani Abdullah (N. Abdullah) is a post-doctoral research fellow at Research Centre for Nano-Materials and Energy Technology (RCNMET), School of Engineering & Technology and Sunway Materials Smart Science & Engineering (SMS2E) Cluster, Sunway University. She obtained her Bachelor (Chemical Engineering) and PhD (Fuel Cell

Engineering) from National University of Malaysia (UKM) in 2013 and 2018. She currently works on the fuel cell & hydrogen technology, energy storage, nanomaterial and catalysis.

Dr. Tan Kim Han is a research fellow for the Research Centre for Nano-Materials & Energy Technology (RCNMET), School of Engineering & Technology (SET), Sunway University, Malaysia. He obtained both Master of Engineering (major in Nanotechnology) and PhD in Advanced Materials & Nanomaterials from University Malaya, Malaysia. He previously worked as a postdoctoral researcher at the RCNMET as well. He currently works on the development of 2D nanomaterials and their property tuning & optimization for energy storage applications.

Professor Saidur Rahman is a Distinguished Research Professor and Head of the Research Centre for Nano-Materials and Energy Technology at Sunway University. Thomson Reuters awarded him as a highly-cited researcher for being among the top 1% of researchers with most cited documents in his research field from 2014 to 2021. He has published more than 500 journal articles and a majority of them are in top-ranking journals, with more than 57,000 citations with an h-index of 125 in Google Scholar. He is currently working on research area of energy storage, fuel cell and hydrogen technology, and solar thermal system.

Mohd Amran Mohd Radzi was born in Kuala Lumpur, Malaysia, in 1978. He received his B.Eng. and M.Sc. degrees in Electrical Power Engineering from Universiti Putra Malaysia (UPM), in 2000 and 2002, respectively, and Ph.D. degree from University of Malaya in 2010.He is currently Professor at Department of Electrical and Electronic Engineering, UPM. He is also attached with Advanced Lightning, Power and Energy Research (ALPER) Centre, UPM. His

research and teaching interests are power electronics, power quality, and renewable energy. He is Member of IET, U.K., and Chartered Engineer.

Suhaidi Shafie is a highly experienced academic and accomplished researcher with an extensive background in electrical and electronics engineering. He obtained his Bachelor degree in Electrical and Electronics from the University of the Ryukyus, Japan in 2000. He completed his M.Sc. and PhD from TUAT and Shizuoka University, respectively, in 2005 and 2008. Currently, he holds the position of Department Head of Electrical and Electronic Engineering and Professor at UPM. Dr. Suhaidi's research focuses on optical devices, circuits, and systems, Solar Cell and Photovoltaic, Sensors, and Analog IC interfacing circuits.

1.0 INTRODUCTION

The growing adoption of green energy technology has resulted in intermittent and fluctuating power generation, combined with current load fluctuations, which raises concerns about the security and sustainability of future electricity networks. To address this challenge, energy storage solutions offer a broad range of technology alternatives to manage power supply and build a more reliable and cost-effective electricity grid. In this section, we present a detailed study of flow batteries, which are currently one of the most effective choices for large-scale energy storage systems being utilized globally. In the 1930s, Pissoort first explored the potential of vanadium redox flow battery (VRFB)[1]. Later, Maria Skyllas-Kazacos and her team at the University of New South Wales (UNSW) pioneered the development of VRFB technology, which satisfies the performance criteria for large-scale energy storage applications, featuring a lengthy lifespan and

outstanding energy efficiency (EE), coulombic efficiency (CE), and voltage efficiency (VE) of around 80% in large installations[2]. In the 1980s, Maria Skyllas-Kazacos reported the first practical proof of dissolved vanadium in a sulphuric acid solution[3], and since then, numerous research groups have contributed to the development of revolutionary membrane, electrode, and electrolyte materials for VRFB technology.

The VRFB is a rechargeable flow battery that stores and supplies energy by conducting redox reactions involving various oxidation states of vanadium ions. The VRFB system comprises several major components, including electrolytes, pumps, and power cells, while the VRFB power cells consist of electrodes, a membrane, bipolar plates, and current collectors[4]. In this paper, the authors present a detailed overview of recent enhancements, challenges and future developments in the electrode component, as it is the key component that determines the performance of the VRFB system. As the energy output of VRFB technology is scalable by manipulating parameters such as the number and size of cell stacks and electrolyte volume, without loss of power or degradation of the energy storage system's health, it has become more established in recent years. Additionally, VRFB technology offers a longer lifespan, low maintenance requirements in the long run, and is free from fire hazards[2, 5]. These advantages make VRFB technology suitable for applications in utilities-related industries, uninterruptible power supply (UPS), grid industry, photovoltaic industry, and wind power industry[6].

This review provides an in-depth examination of the VRFB technology, focusing specifically on the electrode materials, electrocatalysts, synthesis methods, electrochemical performances, oxidization, and characterization methods. The article emphasizes the current difficulties related to the electrodes in VRFB and highlights the wide range of potential applications offered by the technology in growing economic markets. The authors discuss the

potential of emerging nanomaterials, such as MXenes, to enhance the existing electrode materials in the VRFB system. This article aims to enable researchers to track recent development progress and identify improvement steps or routes associated with electrode materials, with the goal of optimizing the efficiency of VRFB by designing or manipulating the electrode materials. The authors explore the high electrochemical activity, redox ability, high surface areas, and functional transition metal surfaces of different types of electrocatalysts in various carbon-based electrodes, as well as the influence of MXene on the performance of VRFBs by providing active sites for redox couples and electrocatalytic activity for the electrodes. Furthermore, the article provides important future indications for improving electrode physico-chemical performance using different electrocatalysts and MXene-derived composites in VRFBs, with different types of modification and uniformity morphologies. Given that electrodes are the critical factor influencing the overall reliability of VRFB, this review underscores the need to address the barriers or limitations caused by the electrode materials.

2.0 VANADIUM REDOX FLOW BATTERY (VRFB)

The VRFB is a rechargeable flow battery that accumulates chemical energy using vanadium ions in various oxidation states[5b]. One key advantage of the VRFB is that it uses only a single electro-active substance, vanadium, which can exist in solution in four distinct oxidation states, eliminating the need for two different electro-active substances [7]. The vanadium is typically dissolved in a solution of sulphuric acid (H_2SO_4), hydrochloric acid (HCl), and a few types of additive materials that are added to each half of the VRFB [8]. The VRFB consist of multiple critical elements, such as the electrolyte, electrodes, membrane, bipolar plates, current collectors, cells, and flow frames[4]. The vanadium anolyte and catholyte are held in distinct tanks, and the half-

cells are separated by an ion exchange membrane. Pumps are used to circulate the electrolytes between the half-cells, as illustrates in Figure 1.

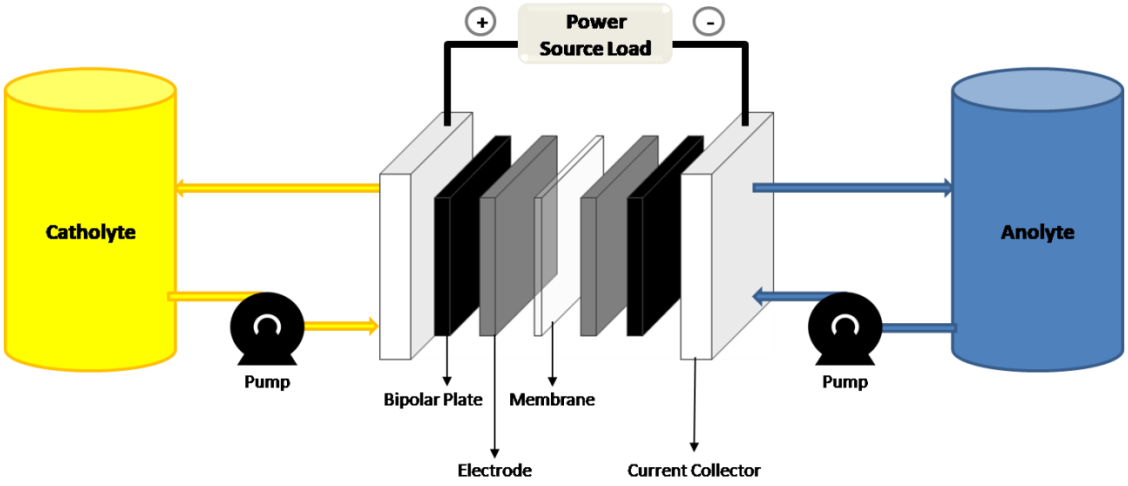

Figure 1: A diagrammatic representation of the VRFB.

Electrical energy is generated in the half-cells by converting chemical energy through the oxidation and reduction of the electrolytes[9]. As the vanadium electrolytes flow through the cell stack, they are transformed from electrical energy to chemical energy[10]. The battery state of charge (SOC) is increased when the electrolytes flow from the cells to the tanks. At the molecular level, V^{3+}/V^{4+} enter the electrochemical cell, as shown in Figure 2. The oxidation of V^{4+} to V^{5+} in the catholyte half-cell is depicted in Figure 2. In this process, the conductive electrode material removes an electron, and an H^+ ion diffuses over the membrane to the other side of the cell[10-11]. Electrons from the external circuit decrease from V^{3+} in the anode half-cell to V^{2+}, with the H^+ ion passing through the membrane to balance the total charge of the half-cell[12]. The two charged electrolytes, V^{2+} and V^{5+}, remain in the half-cells. When the VRFB runs out of energy, it switches to discharge mode, and the two electrolytes in the cell stack, V^{5+} and V^{2+}, convey the chemical energy to it, which is then turned into electrical energy that feeds the external load[10, 11, 13a, 13b]. The charging process occurs in reverse at the molecular level, where an H^+ ion crossing the ion-

conductive membrane releases an electron to balance the charge of the H^+ ion [14]. When the cell is discharged, the electrolytes V^{3+} and V^{4+} exit the cell, and the VRFB supplies electrical power until the electrolytes in the two tanks are completely discharged. Equations (1) - (3) present the chemical reactions that occur during the operation of the cell.

Positive Side: $VO^{2+} + 2H+ + e^{-} \leftrightarrow VO_2^{+} + H_2O$ $E^0 = 1.00$ V (1)

Negative Side: $V^{3+} + e^{-} \leftrightarrow V^{2+}$ $E^0 = -0.25$ V (2)

Overall reaction: $V^{3+} + H_2O + VO^{2+} \leftrightarrow V^{2+} + 2H^{+} + VO_2^{+}$ $E^0 = 1.25$ V (3)

The concentration of V^{2+} to V^{5+} ions in VRFB electrolytes typically ranges from 1 - 2 M, while H_2SO_4 and HCl concentrations are usually between 3 - 6 M and 4 - 8 M, respectively[9a, 15]. The solubility of vanadium ions is significantly influencedby the electrolyte's H_2SO_4 concentration and temperature. Increasing H_2SO_4 concentration decreases the solubility of V^{2+}, V^{3+}, and VO^{2+} but increases the solubility of VO_2^{+}. Conversely, decreasing the temperature of the electrolyte can increase the solubility of other vanadium ions[16]. Vanadyl sulfate ($VOSO_4$), vanadium trichloride (VCl_3), and vanadium pentoxide (V_2O_5) are among the vanadium compounds that have been considered for use in various supporting solutions, such as hydrochloric acid (HCl), sulfuric acid (H_2SO_4), and sodium hydroxide (NaOH)[17]. However, the use of HCl and VCl_3 can generate chlorine gas, while the use of V_2O_5 leads to poor solubility. The concentrations and electrochemical activities of vanadium ions significantly impact the densities and efficiencies of VRFBs. Impurities in the vanadium electrolyte can affect the reaction kinetics, energy density, and stability, as well as the efficiency of the VRFB. Thus, further research is needed to gain a more comprehensive understanding on the nature and effects of impurities in vanadium electrolytes.

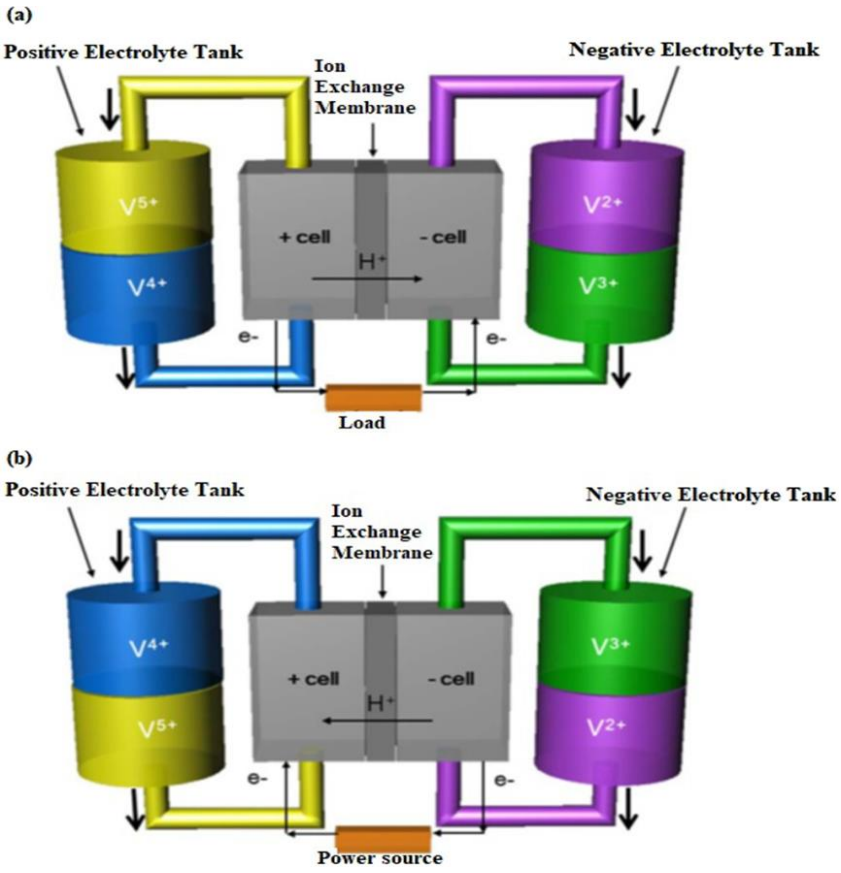

Figure 2: Schematic diagram of VRFB (a) charging and (b) discharging process. Reprinted from publication[10], Copyright (2022), with permission from Elsevier.

An optimal electrode material for VRFBs should possess excellent electrical conductivity, good mechanical properties, great chemical resistance, a reasonable cost, and a prolonged lifespan even under highly oxidizing conditions. Carbon-based composites or inert metallic materials are often used for VRFB electrodes. However, during discharge and corrosion, metal ions can dissolve into the electrolyte from metallic electrodes, resulting in unstable redox potentials and disrupting the VRFB's chemistry. Therefore, metallic electrodes are often made of noble metals with high electrochemical stability or catalytic properties. Early experiments aimed to introduce diverse oxygen functional groups onto electrode surfaces. Nevertheless, subsequent investigations indicated that OH- functional groups were better in providing active sites for vanadium redox pair

processes, thereby increasing electrode reactivity and wettability. While graphite and carbon felt will remain to be the primary electrode materials for VRFBs, future research will focus on "zero-gap" cell architecture to improve reaction kinetics, increase densities, and ultimately improve VRFB stack efficiencies.

The membrane plays a crucial role in the VRFB system, acting as a separator that prevents physical mixing of vanadium ions and self-discharge reactions[14]. Cross-permeation of charged vanadium ions between solutions during oxidation and reduction processes results in significant cell performance degradation. The formation of VO_2^+ on the positive side and V^{3+} on the negative side through undesirable vanadium ion cross-flow[18] prolongs charging and speeds discharging, reducing VRFB efficiency. To be effective, ion exchange and anion exchange membranes must exhibit strong ion conductivity, superior chemical and mechanical durability and low vanadium ion permeability. Although Nafion is well-known for its chemical stability and proton conductivity, its high vanadium ion permeability hinders widespread adoption by intensifying the self-discharge process and resulting in significant capacity and CE loss during long-term operation[19]. Various hydrocarbon-based proton exchange membranes, including poly(ether ether ketone) (PEEK)[20], poly(fluorenyl ether ketone sulfone)[21], poly(arylene ether ketone) (PAEK)[22], porous polytetrafluoroethylene(PTFE)[23], and poly(arylene ether ketone) with imidazole (PAPI)[18], have been investigated as Nafion alternatives. However, the ion transport process across VRFB membranes is challenging[24] because protons migrate with sulphate anions through free volume or acid molecules absorbed in membranes[25]. Furthermore, compared to proton exchange membranes, hydrocarbon-based membranes have weaker redox stability, particularly on the positive half-cell side[26]. Therefore, membrane fabrication research focuses on improving ionic conductivity, mechanical characteristics, chemical stability, and vanadium ion permeability.

The term "current collector" in the literature is used interchangeably, with some studies referring to copper plates at each end of the stack[27], while others relating it to bipolar plates (BP)[28]. The BP is a versatile and necessary component of the VRFB system, serving several functions such as electrically connecting and chemically separating each cell, providing stack support, and allowing electrolyte distribution in the porous electrode through the flow field, similar to the fuel cell system[15c, 29]. The BP should possess excellent electrical conductivity to facilitate efficient charge transfer, good mechanical properties to provide structural support, good corrosion resistance to maintain electrochemical stability, no electrolyte leakage to avoid mixing, and be composed of materials that are widely available at reasonable costs[30]. Materials used for BP fabrication are susceptible to corrosion, swelling, electrolyte leakage, and interfacial contact resistance, posing challenges for their application.

3.0 POTENTIAL APPLICATION AND MARKETS OF VRFB TECHNOLOGY

3.1 Potential Application of VRFB

VRFB technology offers numerous advantages, making it a promising large-scale energy storage system. A significant benefit of the VRFB technology is its scalability, where the power output can be adjusted by altering the size and number of cell stacks[31], and the energy capacity can be determined by the amount of the stored electrolyte[32]. Additionally, VRFB eliminates power or capacity loss due to side reactions in the electrolyte solution, ensuring a longer lifespan than conventional batteries even after deep discharge[33]. Unlike other flow batteries, VRFB utilizes vanadium in both electrolytes, preventing battery degradation through cross-contamination[33]. In laboratory settings, VRFB has demonstrated a lifespan of up to 20,000 cycles with 70% to 90% efficiencies, far exceeding the typical 4,000-5,000 cycles of solid-state batteries[5a, 34]. The

technology also boasts a rapid response time, can operate at 0% charge, and has low maintenance requirements[2, 5b, 5d]. VRFB provides additional benefits such as frequency regulation, peak and base load shifting, and reliable operation[7, 10]. Furthermore, it offers a sustainable and safe package due to its ability to reuse and recycle electrolytes and its stable aqueous electrolyte chemistry, which eliminates the risk of fire hazards[5c].

All of these advantages make the VRFB adaptable for use in various utilities-related industries, which involve the generation, supply, or utilization of electricity, such as electrical apparatus, renewable integration, utility services, and others. According to data from Data Intelo[35], the largest percentage of VRFB end-users is in the UPS application, accounting for 62.5%, followed by the wind power industry (18.7%), utility facilities (11.4%), photovoltaic industry (3.1%), and others (4.2%). The UPS application serves as an emergency power supply during power outages, where the VRFB system acts as a battery bank that stores electrical energy and supplies it during an emergency[36]. Therefore, rapid response time is a critical property required for this application. In the renewable integration industry, the VRFB technology is mainly used as an energy storage system that is connected with renewable generators, such as wind and solar power generation farms. Energy storage plays a significant role in ensuring the stability of the power grid in the quest for 100% renewable energy[37]. This energy storage method maximizes the use of energy generated from renewable sources and delivers it continuously[38]. The VRFB energy storage system is also a promising solution for the grid industry, specifically in smart-grid or micro-grid electricity network applications. The grid that is connected to the VRFB energy storage system can provide multi-ancillary services, effectively regulating frequency and performing peak-shaving services due to its fast response time advantages[7]. Additionally, this system guarantees economic feasibility and capital cost reduction in grid infrastructure[6].

The widespread adoption of VRFB technology in various applications is a testament to its effectiveness and practicality. The technology has been in use for several decades, with notable installations including a 12kWh VRFB system in a solar-powered home in Thailand and a grid-connected VRFB load levelling system at the Kashima-Kita Electric Power station in Japan[5d]. Industry players such as Sumitomo Electrics Industries (SEI) have also deployed VRFB systems for emergency power supply, peak shaving, solar and wind integration, UPS, micro-grid and other applications[39]. Moreover, SEI and Hokkaido Electric Power Inc. (HEPCO) installed one of the world's largest VRFB systems at the Minamihayakita Transformer Station in Abira-chou, Hokkaido, Japan[40]. Dalian Rongke Power has delivered 20 VRFB projects across China, Germany and the United States, while Pu Neng has completed more than 20 VRFB projects in Asia, Africa, Europe and the United States[5c]. Furthermore, many other global industry players such as Schmid Group, Voltstorage, Volterion from Germany, RedT Energy from the United Kingdom, UniEnergy Technologies from the United States, and others are also developing VRFB technology.

3.2 VRFB Markets

The growth of the industrial sector and the increase in global population have led to a significant rise in energy consumption, resulting in the growth of the utilities-related industry worldwide. The adaptability of VRFB technology in various applications within this industry is a key factor driving the expansion of the global VRFB market. As stated in the market report on VRFB by Reports and Data[41], the market size was large in 2019 and it is projected to expand significantly in the next 10 years. The Asia Pacific region (China, Australia, India, South Korea, Japan, etc.) is the largest global VRFB market due to large-scale application in utility facilities, clean energy integration, and UPS systems. Figure 3 presents the prospect and cost breakdown for the VRFB system. The

prospects for VRFB technology from 2018 to 2030 involve three main commercialization indicators: performance, durability, and cost. The performance of VRFB technology is expected to improve in the upcoming years, while the durability and cost of the VRFB system are anticipated to decrease by 50% from 2018 to 2030[42]. These prospects can be realized through progressive research, particularly in developing new material components, optimizing battery performance, and enhancing VRFB efficiency.

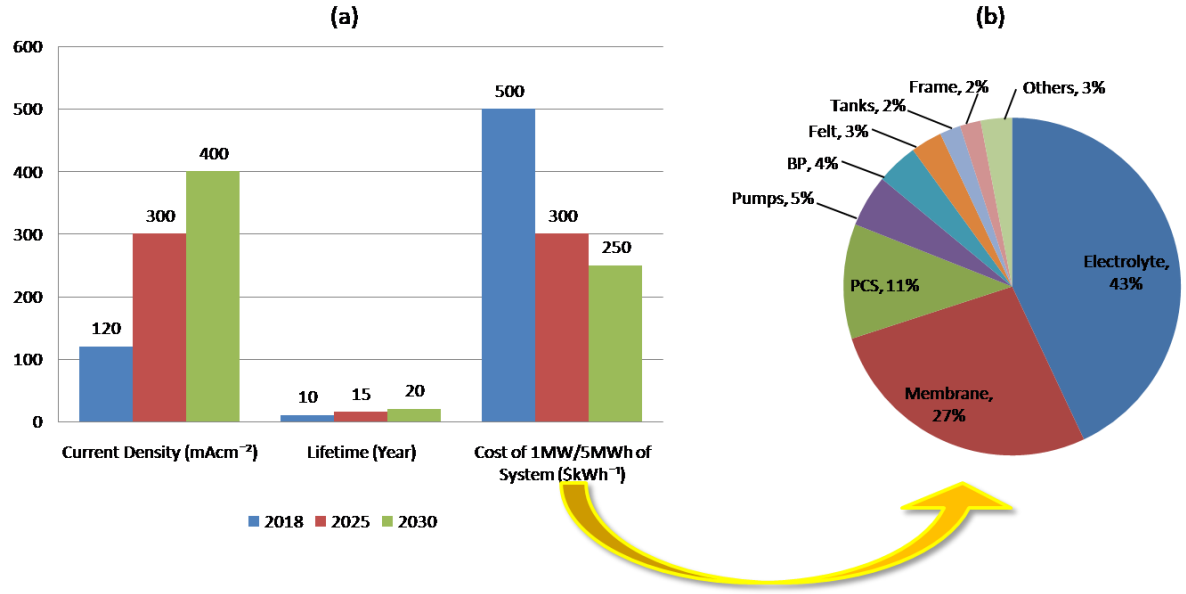

Figure 3: (a) Prospect for the VRFB technology from 2018 to 2030, (b) Cost breakdown for the VRFB system.

The cost of VRFB systems can be broken down into three categories: investment, operating, and energy costs, with investment costs accounting for the largest portion at almost 87% of the total cost[43]. The VRFB stack system is one of the components contributing to the investment cost, and the cost ratios of each component in the VRFB stack system are shown in Figure 3 (b). The electrolyte component makes up the largest portion of the VRFB system cost at 43%, followed by the membrane and power conditioning system (PCS) at 27% and 11%, respectively[44]. The electrolyte component is costly primarilyis due to the expensive vanadium

market price. However, the urgent global need for large-scale VRFB technology to achieve carbon neutrality and the global carbon peak has made industrialization development a priority, and this is expected to reduce the price of raw materials in the next 5 – 10 years[44]. Despite the relatively high cost of VRFB technology, its long service life of up to 15 – 20 years makes it a cost-effective and profitable technology option for investors[37, 43].

4.0 ELECTRODE MATERIAL IN VRFB

The electrodes play a critical role in VRFBs and are typically made of carbon-based materials such as GF, CF, and CP, due to their low cost, strong conductivity, and high stability in acidic environments[45]. Each material has their own roles or benefits for VRFBs. For example, GF have high specific surface area; enhance the adhesion between the deposited metal oxide catalysts electrode stabilization preventing capacity loss and stable catalytic effect[46].The electrochemical reversibility and activity of V^{2+}/V^{3+} and VO^{2+}/VO_2^{+} redox couples on GF can be enhanced significantly by the anodic potentiostatic polarization approach due to the introduction of C=O and COOH groups but it is costly than CP and CF. When compared to other metals that would potentially be suited for large-scale applications, CF is the most prominent electrode material due to its low cost and high corrosion resistance[47]. It exhibits a high overpotential towards the hydrogen evolution reaction (HER), which is a potential parasitic reaction in the negative half-cell. CP have a large surface area, high conductivity, excellent stability, and an increasing number of functional groups to enhance their electrochemical activity toward vanadium redox couples, electrode/electrolyte interaction, and mass transport resistance[48]. Vanadium ions diffuse from the bulk electrolytes to the region of the electrodes and are absorbed on the electrode surfaces. Through the interchange of functional group hydrogen ions, the absorbed vanadium ions are coupled to the

electrode. Only the electron transfer process occurs in the VO^{2+}/VO_2^{+} redox pair, whereas only the oxygen transfer reaction occurs in the V^{2+}/V^{3+} redox couple. At the positive electrode, an oxygen atom of the C-O functional group travels to the VO^{2+}, and an electron of the VO^{2+} is transferred to the electrode via the C-O-V bond, increasing the vanadium ion's oxidation number from +4 to +5. At the negative electrode, one electron is transferred from the electrode to the V^{3+} via the C-O-V bond, reducing the vanadium ion's oxidation number from +3 to +2. The ion exchange process takes place between the V ion connected to the electrode surface and the H^{+} ion in the electrolyte, and the thus produced reactants (VO_2^{+} and V^{2+}) diffuse back into the originally formed electrolytes[13a]. Electrodes need to provide active sites for electrochemical reactions to occur through ion exchange and electron transfer mechanisms. However, the limited diffusion of vanadium ions to active sites and insufficient electrochemical activity of electrodes for desired reactions are significant challenges to achieving optimal VRFB performance[49]. In particular, the anode (V^{2+}/V^{3+}) has a slower redox chemistry than the cathode (VO^{2+}/VO_2^{+}) on electrodes[47, 50], which is a rate-limiting factor in high-performance VRFB operation. As electrolyte ion redox reactions occur on the electrode's surface, the electrode material is a crucial factor in the battery's overall performance. In the following section, we will discuss some of the most critical requirements for an electrode to achieve optimal VRFB performance. Although the electrode does not participate in the redox processes, it must serve as a source of active sites for the redox pair. Furthermore, the electrode must be chemically and electrochemically stable to perform well in an acidic medium and within the battery's working potential window. Additionally, the electrode must have high electrical conductivity to facilitate rapid charge transfer. The electrode is a critical factor in flow battery output and power density as it provides an electroactive surface area and conducts electrons[51].

Carbon-based materials like GF, CF, and CP are commonly used as electrode materials in VRFBs because they fulfil most of the requirements[52]. However, most research has used the same material for both the anode and cathode, and there have been few studies with different electrode materials for each half-cell[53]. For instance, Maleki et al.[53b] used commercial felt on the positive side and carbonized electrospun material with commercial CF on the negative electrode. GF is the most frequently used electrode material due to its high electrical conductivity, good chemical stability, large specific surface area, and a wide potential activity window. Despite its advantages, insufficient electrochemical activity and poor hydrophilicity lead to a low number of active sites for redox couples and low electrolyte accessibility, which impedes the development of VRFB technology. Researchers have explored various electrode modifications using metals or metal oxides such as Pt, Pd, Bi, Fe, Cu, PbO_2, WO_3, Mn_3O_4, ZrO_2, NiO, $CuPt_3$, and Nb_2O_5, as well as carbon-based, carbon metal-based, and carbon-metal composite-based catalysts[52a, 54]. The advantages and drawbacks of some of these materials are shown in Figure 4.

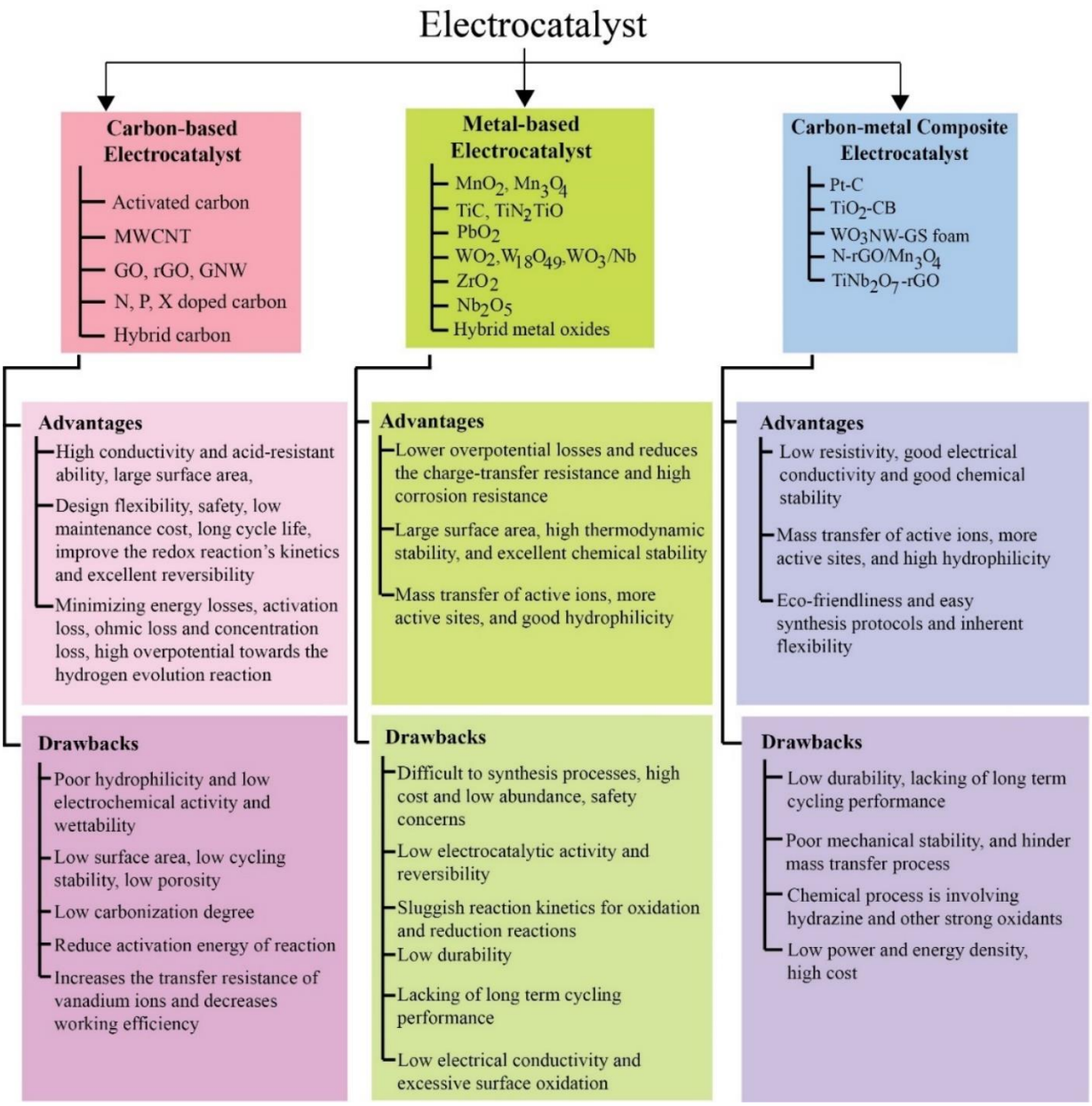

Figure 4: Electrocatalysts for VRFB.

Table 1: Recent development of modified or activated electrodes for VRFBs system.

Electrode material	**Catalyst**	**Synthesis Method**	**Findings**	**Ref.**
GF fiber	N-doped carbon nanospheres	Chemical treatment	Excellent EE, capacity retention, and wettability in an electrolyte. Provide long cycles at 150 $mAcm^{-2}$ current density, and adaptability in wide range of working temperatures.	[55]
CF	Benzoyl peroxide	Chemical treatment	Improved EE of 75% at 100 $mAcm^{-2}$ current density. Enhancement of the electrocatalytic properties of oxygen-functionalized surfaces.	[56]
GF	P-doping	Hydrothermal	Excellent electrochemical activity, reversibility, electrolyte wettability, and durability (over 1000 cycles). Adaptability in broad range of working temperatures (-20^{o}C – 60^{o}C).	[57]
GF	$KHCO_3$-activated carbon microspheres	Hydrothermal	Excellent electrocatalytic activity, and enhance EE and discharge capacity at high current density.	[58]
GF	Polymer of tubular polypyrrole	Heat treatment	Electrochemical activity reversibility was increased and enhanced the discharge capacity. Improved performance with the EE (82.20%) at 80 $mAcm^{-2}$.	[59]
GF	Rayon-based & PAN-based	Thermal treatment	Rayon-based felt have a consistent performance during the entire testing period, while PAN-based showed exhibited persistent and severe deactivation.	[60]
CP	rGO & Graphene	Passive deposition on the electrode	The rGO deposition has excellent kinetic performance compared with graphene. The enhancement of electrochemical kinetics was observed, while the negative impact on mass transfer properties was not significant.	[61]
Melamine foam electrode	3D N, P co-doped/ rGO coated carbonized melamine	One-step foaming method	rGO can enhance conductivity and specific surface area. N and P atoms provide extra sites for redox reactions. Excellent EE (74.14%), long-term cycling stability and charge-discharge cycles at 200 $mAcm^{-2}$ without significant degradation.	[62]
ECNF	Graphite nanopowders	Physical procedures to reach the composite	Significant increment on electrochemical activity. Increasing the content of nanoparticles led to an increase in the reversibility of vanadium species.	[63]
CP		KOH activation	Improvement in active sites and electrolyte flowrate leads toward the high performance of VRFB.	[64]
CP		Pseudo-channel effect	Enhanced the overall active surface area of the electrodes.	[65]

			The EE of the laser-punched holey CP electrode was 85.11%, which is a 10.41% increase compared to pristine CP.	
CF	SnO_2 nanoparticles	Hydrothermal	Improved performance stability, EE (77.3%) in high current density, enhanced discharge capacity (23.7%) and retention capacity.	[66]
GF		Acidic treatment	Lower peak potential separations, less charge transfer resistances, and higher peak current densities, charge/discharge capacities and EE compared to typical thermal treatment.	[67]
CF	MWCNT	Solution deposition method	Significantly enhanced electrolyte reversibility and electrochemical activity, while increasing the CE and EE.	[68]
GF	PAN-based		Utilizing the electrocatalytic properties of antimony in stabilizing the electrode. Facilitating redox reactions improving battery CE, VE and EE.	[69]
PAN-based GF	Nitrogen carbon nanofiber (NCNF)	N-doping procedure	Increased electron and ion transfer, improved surface defect, and enhanced hydrophilicity and conductivity. Excellent battery performance and discharge capacity.	[70]
CF	Graphene	Solution coating method	High peak current, low polarization and potential difference, and enhanced VE and EE.	[71]
Graphite fiber mat		Thermal activation	Reduced the polarization resistance (23%) of VRFB. The EE is 80% at 100 $mAcm^{-2}$.	[72]
GF	Carbon nanoparticles	Four-step procedure	High surface area, increased electrocatalytic activity and decreased ohmic loss, which enhanced EE up to 84.8%.	[73]
GF	Copper nanoparticles	Solution coating method	Significant enhancement in electrochemical activity, EE (17%) and electrolyte utilization (53%).	[74]
CF	Mesoporous tungsten oxide and oxynitride		The oxynitride catalyst has high VE, specific capacity, and surface area, and exhibits low current transfer rate and capacity loss.	[75]
CF	Boron-doped mesoporous graphene	Hydrothermal	The surface-active sites for redox activity were enhanced, leading to a notable improvement in the kinetics and reversibility of ion. EE increased 17.3% at 150 $mAcm^{-2}$.	[76]
GF	Titanium nitride nanowire	Hydrothermal	Enhanced EE (43.3%) and electrolyte utilization (15.4%). Significantly improved in active sites and electrochemical activity.	[77]
Carbon cloth		KOH activation	Increased surface area, EE (80%) and electrolyte utilization (74.6%).	[78]
GF		Water activation	The VRFB demonstrated a CE of 95.06%, a VE of 87.42%, and an EE of 83.10%.	[79]
CF	Bi nanoparticle	KOH-etched treatment	Increasing the concentration of oxygen functional groups (16.49%), resulted in a decrease in charge transfer resistance and an improvement in EE by 36.2%.	[80]

ECNF	PAN/DMF based	Hydrothermal	The mass transfer kinetics, electrochemical reaction area, and electrocatalytic activity were enhanced. Efficiencies and power density of VRFBs are highly improved.	[81]
CF	Nd_2O_3 nanoparticles	Chemical treatment	Greatly enhanced EE and charge capacity.	[82]
GF	Mn_3O_4/MWCNT	Solvothermal method	Higher discharge capacity, lower electrochemical polarization, and enhanced EE by 3.73%.	[83]
CNF	PAN and PVA-based	Four-probe procedure	Enhanced transport properties and increased the specific surface area. Achieved high peak power density (~1.9Wcm^{-2}) and EE (79.3%) at 400 $mAcm^{-2}$.	[84]
ECNF	CeO_2 nanoparticles	Electrospinning and carbonization method	Enhanced electrochemical surface area by four times. Improved electrocatalytic activity of the negative side, discharge capacity and EE.	[85]
CNF	ZrO_2 nanoparticle	Electrospinning method	Excellent capacity retention (95%), enhanced EE (8.3%) and discharge capacity (8.7%).	[86]
GF	Cr_2O_3	Impregnation method	Significantly improved VE, EE and discharge capacity up to 75.9%, 67.6% and 83.6%, respectively.	[46]
CNF	TiO_2 nanoparticles	Electrospinning method	Enhanced EE by 8.7% and increased discharge capacity by more than 50%.	[87]
CP	MWCNT	Flowing deposition	70% increment on power output.	[88]
CF	Mesoporous carbon	Acidic treatment	Excellent EE compared to the bare CF.	[89]
Nanoporous carbon scaffold	Mesoporous carbon	Heat-treated	Increased the mass transfer rate, and the utilization of electrode surface area, low overpotential.	[90]
Polyacrylonitrile and poly methyl methacrylate	PAN based	Electrospinning	81.03% EE at 200 $mAcm^{-2}$, long-term cycling stability.	[91]
Glassy carbon	SnO_2/rGO	Sol–gel	EE increased 69.8%, boosted charge transfer, and electron transport processes.	[92]
GF	metal-organic framework	Carbonization techniques	Improved EE 75%, increases the capacity.	[93]
N-doping on carbon cloth skeleton	Polyethyleneimine	Pyrolysis method	Higher electrochemical activity towards vanadium species, improved VE, CE, EE.	[94]
Aligned carbon fibers	PAN-and PVA-based	Electrospinning	EE 79.3% at 400 $mAcm^{-2}$, high peak power density.	[84]

The modification of electrodes using different types of electrocatalysts and their application in VRFBs is summarized in Table 1. The table reveals that many studies have been conducted to enhance the efficiency of VRFBs by increasing the electrode's surface area and electrochemical active sites for redox reactions. These methods are recognized for their ability to introduce functional groups and/or other metallic electrocatalytic elements, particularly during charge-discharge cycles, which provide active sites for vanadium ion reactions. The synthesis of the catalyst involved several processes, such as thermal, hydrothermal, acid, and Fenton's reagent. Oxygen functional groups such as C-O and C==O, and other functional groups such as $-NH_3$ or $-SO_3H$, were added to the carbon-based electrode. Carbonaceous materials, including graphene, multi-walled carbon nanotube (MWCNT), and nitrogen doping (N-doping) or phosphorus doping (P-doping) materials, were used to increase the number of functional groups and the electrode's surface area as a catalyst to promote the redox reaction.

Two key approaches have been utilized to enhance VRFBs: electrode activation and surface modification techniques. The activation technique requires the introduction of functional groups to increase the number of electrode sites. Surface modification techniques have been implemented through three mechanisms: (1) increasing the surface area and active site concentration for redox reactions, (2) enhancing the electrode's porosity to increase hydraulic permeability and facilitate electrolyte transport, and (3) reducing ion concentration loss and pumping capacity. Researchers have utilized various carbon-based, metal-based, and carbon-metal composite materials for VRFB electrodes, as summarized in Figure 5, and have presented significant improvements in their work through the use of different types of electrocatalysts.

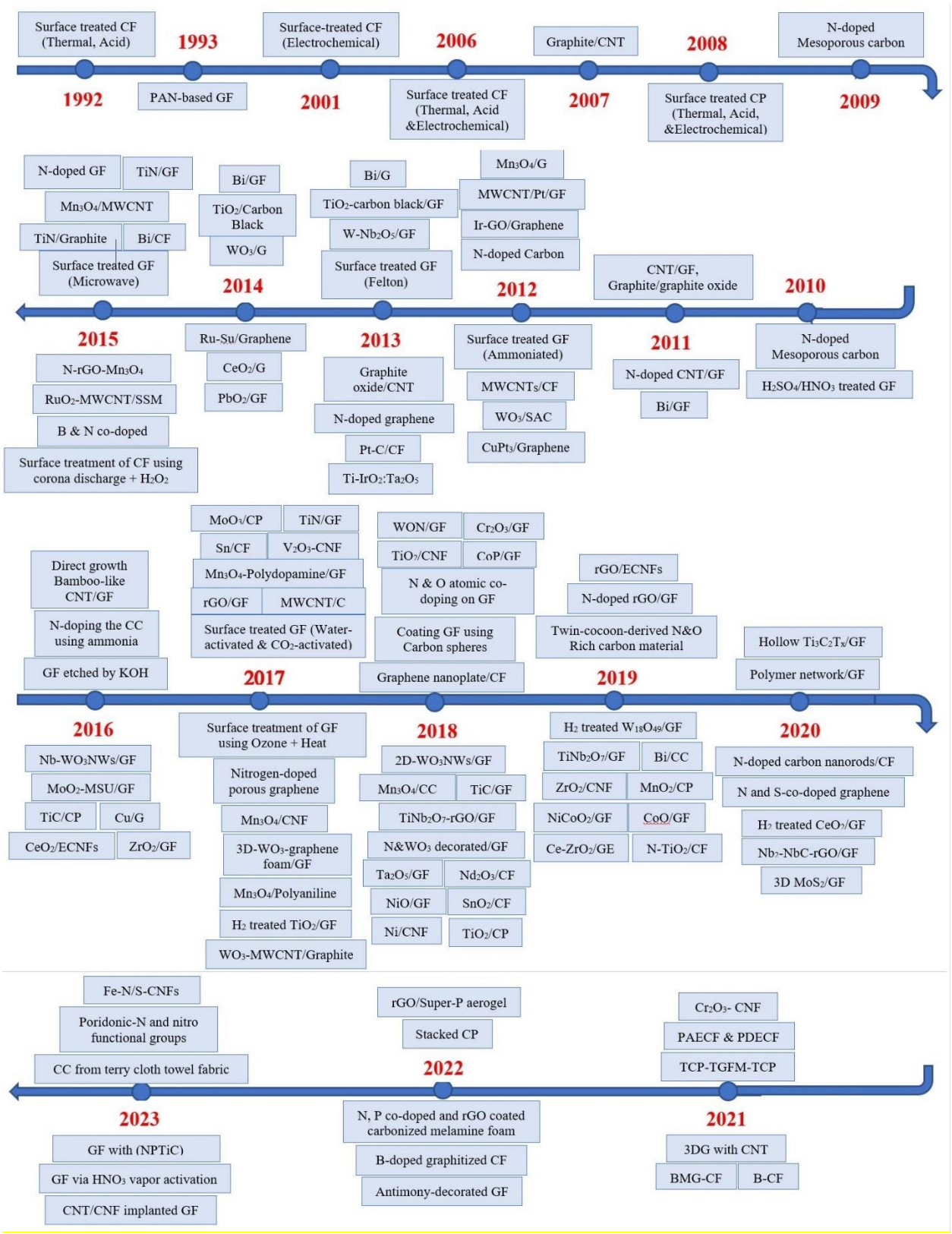

Figure 5: Timeline for research on different types of electrode materials for the VRFB.

4.1 Graphite Felt

Table 2: Recent advances in GF electrodes with different types of catalysts in VRFB.

Catalyst	Deposition Method	Current Density ($mAcm^{-2}$)	Electrolytes	VE (%)	CE (%)	EE (%)	Cycling Stability (Cycles)	Ref.
AC (sugarcane)	-	100	2M $VOSO_4$ + 5M H_2SO_4	77	94	72	50	[95]
Phosphoryl-ethylamine	Dip Coating	120	1.5M $VOSO_4$ + 2M H_2SO_4	83.8	-	79.4	35	[96]
Hydroxyl MWCNT	Dropping	80	1M V-ion+ 4.2M H_2SO_4	83	96	79.7	50	[97]
Carbon foam	Spraying	40	1M $VOSO_4$ + 1M H_2SO_4	88	90	79	10	[98]
N-CNT (Fe)	Pyrolysis	100	0.1M $VOSO_4$ + 3M H_2SO_4	83	96	81	30	[99]
MnO_2	Hydrothermal	150	0.75M $VOSO_4$ + 3M H_2SO_4	79	95	75	120	[100]
α-TiO_2	Dipping	100	0.8M V-ion+ 3M H_2SO_4	74	98	72.5	50	[101]
Ta_2O_5	Hydrothermal	80	1.6M $VOSO_4$ + 2.5M H_2SO_4	78.1	94.8	73.7	100	[102]
PbO_2	Pulse electro-deposition	70	0.5M $VOSO_4$ + 3M H_2SO_4	82.4	99.5	82	30	[103]
CeO_2	Precipitation	200	2M $VOSO_4$ + 2M H_2SO_4	85	92	78	100	[104]
Nb_2O_5	Hydrothermal	150	2V $VOSO_4$ + 5M HCl	90	74	73	16	[105]
WO_3	Hydrothermal	70	1M $VOSO_4$ + 3M H_2SO_4	88.6	99.1	87.8	20	[106]
ZrO_2	Immersion-precipitation	200	1.5M V-ion +3M H_2SO_4	71.9	93.7	67.4	200	[107]
WO_3-NWs/ GS foam	Dropping	80	1.6M $VOSO_4$ + 2.5M H_2SO_4	83.6	94.9	79.4	50	[108]
$TiNb_2O_7$-rGO	Ink-dispersion	120	1.6M $VOSO_4$ + 2.5M H_2SO_4	82.7	96.3	79.7	200	[109]
PDA-Mn_3O_4	Polymerization	150	0.7M V-ion + 2.5M H_2SO_4	61.5	99.3	61.1	50	[110]
TiC	Hydrothermal	100	1.6M V-ion + 4M H_2SO_4	75	-	75	20	[53a]
Nb-doped TiO_2	Heat-treated	40	0.15M V-ion + 3M H_2SO_4	96	98	95	100	[111]
NTiC	Mechano-chemical	30	2M V-ion + 3M H_2SO_4	58.9	98.9	57.9	50	[112]
Antimony	-	60	1.2M $VOSO_4$ + 1.5M H_2SO_4	95	88	75	10	[69]
NiO	Calcination	60	1.6M V-ion + 3.5M H_2SO_4	89	98	87	50	[113]

Although GF is currently the most popular electrode material for VRFB systems due to its high surface area, chemical stability, and electrical conductivity, it alone cannot guarantee high cell performance. Thus, further research is needed to optimize its use in this system. To address this, numerous advancements have been made for GF-based electrodes, which are summarized in Table 2. One way to enhance electrodes is by introducing functional groups to their surface through doping and activation techniques. One such method involves controlled doping and removal of oxygen species through thermal oxidation and reduction of GF electrodes to improve their vanadium redox kinetics[114]. To achieve this, temperature-programmed oxidation and reduction techniques were utilized to regulate the reductive deoxygenation and thermal oxygen doping of GF electrodes. Research on the electrocatalytic properties of GF electrodes suggests that the surface defects of carbon electrodes, rather than oxygen functionalities, are the most important active centers for intrinsic vanadium redox kinetics in both the positive (VO^{2+}/VO_2^{+}) and negative (V^{2+}/V^{3+}) reactions in flow batteries[115].

Significant efforts and research have focused on introducing abundant oxygen functional groups onto GF electrodes through various ways such as acid treatments, thermal doping, electrochemical oxidation, and plasma irradiation[116]. However, excessive oxygen functional groups can increase resistance, negatively affecting electrode responsiveness. To improve GF performance, Wang et al.[115] used a combination of HF etching and H_2O_2 hydrothermal treatment. The etching grew more severe after reacting with H_2O_2, resulting in a large number of particles distributed across the GF surface. He et al.[117] modified GFs to have uniform surface nano-cracks, providing improved pathways for electrolyte flow and reaction kinetics, leading to a higher EE of 87.0% at 30 $mAcm^{-2}$, 4.2% larger than that for pristine GF. Additionally, Chang et al.[118] used CO_2-activated GFs in the electrodes, achieving higher CE, VE, and EE values of 94.52%, 88.97%,

and 84.15%, respectively, compared to untreated GF and N_2-activated GF VRFBs. N-doping is also an important recent advancement in GF, as the VRFB system with activated GF yielded an EE of 89.6%, and N-doped alkaline GF yielded 87.4% at a current density of 50 $mAcm^{-2}$, which is a significant improvement over untreated GF, as reported by Gautam et al.[119]. Finally, Hassan et al.[120] used GF in a $K_2Cr_2O_7$ solution with a highly functionalized surface and improved active surface area, enhancing the electro-affinity of GF against vanadium due to C-O groups and the reversibility of vanadium (V) reduction. Liu et al.[111] used Nb-doped TiO_2 (NTO) to a heat-treated graphite felt and found EE of 82.03%, which is 6.2% higher than that of pristine GF. Mohan et al.[112] Mechano-chemical technique, nano-titanium carbide (NTiC) found CE 98.89% and EE 57.9% after 50 cycles at 30 $mAcm^{-2}$. Applying calcination heat treatment in GF electrode, Uan et al.[113] found VE 89%, CE 98%, EE 87% after 50 cycles.

Researchers have found the deposition of electrocatalytic materials on GF electrodes to be highly effective in maximizing cell performance, with materials including carbon-based, metal-based, and carbon-metal composites being widely explored. Dai et al.[121] treated CNTs with KOH and discovered their strong catalytic effect on VO^{2+}/VO_2^{+}. González et al.[122] synthesized graphene-modified GF and achieved a high EE of 95.8% for the VRFB cell at 25 $mAcm^{-2}$, improving the wettability of the electrode and its active area toward vanadium redox reactions. Additionally, the water activation method has been utilized to increase the electrochemical activity of GF[79].

rGO is a carbonaceous material that possesses high electronic mobility as well as thermal and electrochemical stability, making it an attractive candidate for catalytic reactions during VRFB operation and for ensuring extended cycle life of the catalyst. Moreover, N-doped reduced graphene oxide (N-rGO) has been found to have greater catalytic activity[123], with the amount of

N-doping having a significant impact on its performance, as suggested by Jin et al.[124]. Using urea as the nitrogen source, Shi et al.[125] synthesized N-doped graphene, pyrolyzed at 900 °C. The result exhibits good electrochemical performance and enhanced the electrochemical reversibility and catalytic activity for the VO^{2+}/VO_2^+ reaction. Catalysts for the VO^{2+}/VO_2^+ redox reaction include microcrystalline cellulose-derived N- and P-co-doped carbon and diammonium hydrogen phosphate ($(NH_4)_2HPO_4$). The doping enhances the catalyst's wettability, leading to an increase in the proportion of interfacial area that is accessible for the reaction. Using N- and P- co-doped catalyst-coated GFs increased EE and discharge capacity, particularly at higher current densities, as compared to un-doped GF[126]. Additionally, Gursu et al.[127] reported the formation of P-doped graphene on pencil graphite electrodes, which increased peak currents of the positive electrode reaction, electrochemically active surface area, and peak separation.

The performance of modified GF electrodes using different metal-based electrocatalysts has been investigated by various researchers. Xiang et al.[46] employed chromium oxide as an electrocatalyst and observed improved performance with VE of 75.9% and EE of 67.6% at 150 $mAcm^{-2}$, and an 83.6% increase in the cell's discharge capacity, compared to pristine GF. Wu et al.[103] used pulse-electrodeposition to deposit lead oxide (PbO_2) on GF, resulting in CE, VE, and EE of 99.5%, 82.40%, and 82.00%, respectively, at a current density of 70 $mAcm^{-2}$, with a 11% loss in initial capacity after 30 cycles. Zhou et al.[104] investigated the use of cerium dioxide (CeO_2) (0.1 – 0.5 wt.%) on GFs and found an increased EE of 64.7% at 200 $mAcm^{-2}$, compared to the pristine GF's EE of 53.9%. Shen et al.[106] synthesized tungsten trioxide-modified GF electrodes (WO_3-modified GF) and achieved excellent values of CE 99.1%, VE 86.66%, and EE 87.86% at 70 $mAcm^{-2}$. Kabtamu et al.[128] synthesized Nb-doped hexagonal tungsten trioxide nanowires (Nb-doped h-WO_3 NWs), which resulted in an EE of 78.10% at 80 $mAcm^{-2}$. In another study, Kabtamu

et al.[129] enhanced GF electrodes with $TiNb_2O_7$ nanoparticles, which exhibited high catalytic activity, stability, and increased oxygen-containing functional groups, resulting in an EE of 79.06% at 100 $mAcm^{-2}$, which was 4.43% and 15.73% higher than typical GF and pristine GF electrodes, respectively (see Figure 6).

González et al.[130] utilized nano-dispersed bismuth to modify GF electrodes and reported good electrochemical performance and long-term stability. Wei et al.[74] employed a copper (Cu) catalyst on GF and observed great stability and capacity retention. The Cu metal on the GF surface catalyzed the V^{3+}/V^{2+} redox process, as evidenced by the presence of Cu ions on the positive side of the surface. Ghimire et al. [53a] utilized carbon-metal composite materials as electrocatalysts on GF. They dispersed titanium carbide (TiC) on GF without a binder and found that it improved the catalytic reaction between the negative redox pair V^{2+}/V^{3+}. The negative half-cell displayed a 13% gain in EE at 100 $mAcm^{-2}$, with good stability and high-capacity retention over repetitive cycles. Jiang et al.[131] used bifunctional B_4C as a material for both VRFB electrodes and achieved an EE of 88.9% at 80 $mAcm^{-2}$. Bayeh et al.[109] introduced another carbon-metal-based material combination using $TiNb_2O_7$-rGO on GF electrodes and achieved 83.1% and 70.7% of EE at current densities of 80 $mAcm^{-2}$ and 120 $mAcm^{-2}$, respectively.

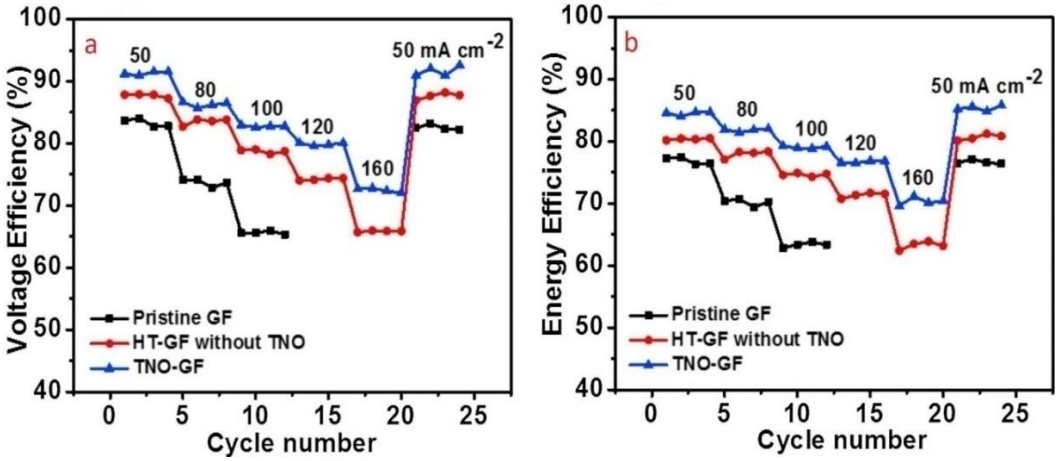

Figure 6: Different electrode's (a) VE, and (b) EE at current densities of 50 to 160 $mAcm^{-2}$.

Reprinted from publication[129], Copyright (2022), with permission from Elsevier.

4.2 Carbon Felt

CF electrodes have been modified with various electrocatalysts[132] and subjected to multiple treatments to improve their electrochemical properties[133]. Despite the material's good electrical conductivity, high surface area, and relative inertness[134], its limited hydrophilicity hinders its reactivity to VO^{2+}/VO_2^+ redox processes in an aqueous solution[135]. The conventional approach of surface modification, such as chemical, thermal, acidic treatments etc., has been used for more than a century to integrate oxygen functional groups onto carbon materials. Table 3 shows the previous studies on the effectiveness of CF electrodes in VRFB with different types of catalysts. One such advancement is electrode surface treatment, which involves attacking the C=C or C-H bonds in CF using BPO to generate free radicals, as demonstrated by Kwon et al.[56]. The resulting BPO-treated CF electrode showed a remarkable EE of 75% at a current density of 100 $mAcm^{-2}$, outperforming the pure CF electrode in the VO^{2+}/VO_2^+ redox process.

Table 3: Recent advances in CF as electrode material with different types of catalyst in VRFB.

Catalyst	**Deposition Method**	**Current Density ($mAcm^{-2}$)**	**Electrolytes**	**VE (%)**	**CE (%)**	**EE (%)**	**Cycling Stability (Cycles)**	**Ref.**
N-CB	Coating	50	2M $VOSO_4$ + 3M H_2SO_4	-	-	82.5	100	[136]
Carboxyl MWCNTs	Dropping	20	1.5M V_2SO_4 + 2M H_2SO_4	91.2	97.5	88.9	-	[137]
ErGO	Potentiostatic	20	0.1M VOSO4 + 2M H_2SO_4	82	-	85	50	[138]
Br-GNP	Ink-coating	50	2M $VOSO_4$ + 3M H_2SO_4	89.5	97	86.8	50	[139]

Graphene nanowall	CVD	25	2.5M $VOSO_4$+ 2.5M H_2SO_4	-	96	90	20	[50]
CNF/CNT	Thermal decomposition	40	2M V_2SO_4 + 3M H_2SO_4	87.5	96.8	85	30	[140]
GO-rGO	CVD	50	1.5M $VOSO_4$ + 2M H_2SO_4	-	-	87	50	[138]
Mn_3O_4	Hydrothermal	40	2M $VOSO_4$ + 2.5M H_2SO_4	91.6	85.7	76.5	20	[141]
Nd_2O_3	Precipitation	100	1.6M V-ion + 2M H_2SO_4	-	71	95	50	[82]
Pt-C	Spray	40	1M $VOSO_4$ + 1M H_2SO_4	89.7	80.6	72.3	10	[142]
TiO_2(α)-CB	Spray	20	3M $VOSO_4$ + 2M H_2SO_4	82.4	90	74.2	-	[143]
MWCNT-ECNF/Bi-ECNF	Electrospun	100	0.1M $VOSO_4$ + 2M H_2SO_4	83	98	82	60	[144]
BPO	Chemical treatment	100	0.2M $VOSO_4$ + 2M H_2SO_4	90	95	75	60	[56]
Boron-doped carbon	Facile thermal treatment	100	-	85	97	80.5	20	[145]
Bio-CF	Rational surface modification	100	0.1M $VOSO_4$ + 2M H_2SO_4	85	-	83.1	150	[146]
N-doped carbon	Electro-deposition	100	1M V-ion + 3M H_2SO_4	94	96	79.2	100	[147]

N-doping in carbon-based materials can enhance VRFB performance by forming ion adsorption sites. Shao et al.[148] synthesized N-doped mesoporous carbon by processing carbon materials in an NH_3 environment, which improved the reversibility of VO^{2+}/VO_2^+. In the past, nitrogen sources such as ammonia gas or ammonia water were used, but Lee et al.[149] employed ethylenediamine in the hydrothermal method to manufacture N-doped material, resulting in a smaller peak potential separation (0.22 V) and excellent electrocatalytic activity. The high concentration of pyroprotein containing N and O functional groups was used by Lee et al.[150] to coat the surface of CF (P-CF), and compared to O-doped and N-doped samples, the synergistic effect of nitrogen and oxygen significantly enhanced the efficiency of the P-CF electrode, especially when pyridyl was present.

Han et al.[151] coated boron-doped carbon onto CF, prepared by the chemical reduction of CO_2 with $NaBH_4$, resulting in a significant decrease in peak separation in the CVs, and improved EE and charge transfer resistance of the positive electrode is reduced. Furthermore, Opar et al.[76] demonstrated that boron-doped mesoporous structures (BMG) exhibit high electrical conductivity, achieving EE of 81.5% (100 $mAcm^{-2}$) and 74.4% (150 $mAcm^{-2}$), which are 9.4% (3.0%) and 17.3% (4.3%) higher than activated-CF and mesoporous graphene-CF electrodes. The BMG also achieve excellent cycle stability, over 100 cycles at 100 $mAcm^{-2}$.Another study presented B-CF exhibits higher energy efficiency (80.56%) at 100 $mAcm^{-2}$ and enhanced redox reactions[145].The chemical treatment method capable to achieve outstanding energy efficiency of 75% at a current density of 100 $mAcm^{-2}$[56].While Lv et al.[147] found excellent discharge capacity of 350 mAh at 250 $mAcm^{-2}$ and EE 79.2% by using carbon nanonetwork wrapped graphite felt electrodes in VRFBs.

According to González et al.[152], the redox activity of graphene oxide (GO) is influenced by various reduction mechanisms that lead to the formation of different functional groups and defects. Thermally reduced GO (TRGO) has an improved graphene structure, low overpotential, and high electron-transfer rates towards the VO^{2+}/VO_2^{+} redox couple. TRGO also exhibits high hydroxyl functional groups and electrical conductivity. Li et al.[138] synthesized electrochemically reduced graphene oxide (ErGO), which showed an 82% increase in VE. Oxygen-based functional groups on the edges and basal plane of graphene were shown to operate as extremely effective redox sites by Park et al.[153]. Graphene nanowalls, which are vertically arranged on a substrate and interconnected with other graphene structures, are another example of graphene-based materials that show promise for VRFB applications.

In the initial stages of VRFBs development, the Skyllas-Kazacos group conducted research on several noble metals including Pt, Pd, Ir, Au, and Mn deposited on CF[154]. Among them, Ir-coated electrodes exhibited the best electrochemical performance, while Pd, Pt, and Au-decorated electrodes showed prominent hydrogen evolution[132, 154]. Wang et al.[132] suggested that H_2IrCl_6 could be converted into metal Ir through heat decomposition, which then binds to the surface of CF. The result show that most of the Ir was still on the CF surface after 50 cycles of charge-discharge trials, proving its great stability in VRFB. Ir-modified CF also improves performance efficiency, lowers the overpotential of the VO^{2+}/VO_2^+ reaction, and lowers battery resistance.

Metal oxides are among the cost-effective metal-based catalysts used for enhancing the performance of CF electrodes in VRFB. Various metal oxides such as Nb_2O_3[82], Mn_3O_4[141], and WO_3[155] have been explored as promising catalysts. Nb_2O_5 exhibited high catalytic activity towards both VRFB couplings, while WO_3 had minimal effect on the electrochemical behavior, and Mn_3O_4 was shown to be soluble in an acidic solution. In comparison to unmodified CF, Kim et al.[141] found that Mn_3O_4-modified CF exhibited excellent mechanical stability and electrocatalytic activity, which improved the redox reaction of vanadium ions and reduced overpotential during charging and discharging. Similarly, Fetyan et al. [82] chemically bonded Nd_2O_3 nanoparticles to CF via a precipitation process, resulting in better performance and a higher discharge capacity and EE. The Nd_2O_3-CF electrode exhibited only a 3% reduction in EE after 50 charge/discharge cycles, while thermally activated CF suffered an irreparable loss of 13%. When spherical TiO_2 nanoparticles for VRFB were investigated by Tseng et al.[143], it was discovered that the hydrophilic TiO2-modified electrode displayed high specific capacitance and energy storage efficiency, low internal resistance, and a sizable electrochemical active area, with EE, VE, and CE of 65.3%, 73%, and 90% at a high current density of 200 $mAcm^{-2}$, respectively.

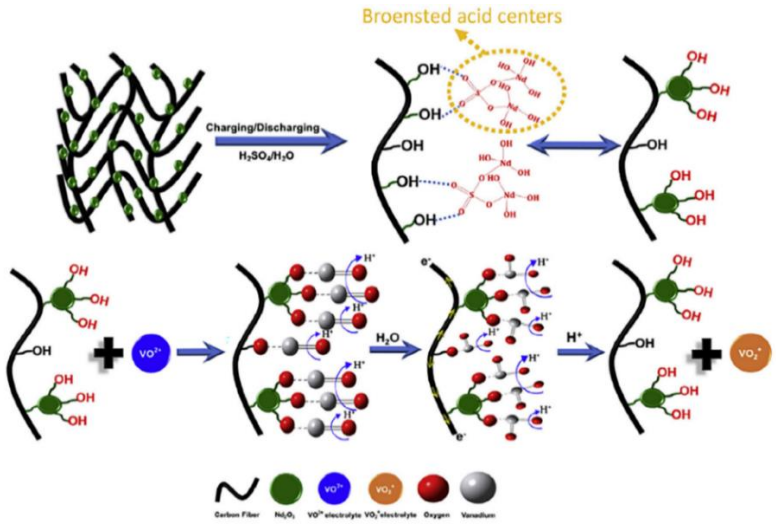

Figure 7: Catalytic reaction mechanism of Nd_2O_3 nanoparticles modified CF. Reprinted from Publication[82], Copyright (2022), with permission from Elsevier..

Performance and electrochemical characteristics of the VRFB have been demonstrated to be significantly influenced by the combination of carbon- and metal-based catalysts. Jeong et al.[142] synthesized polyol platinum on carbon (Pt/C) catalyst using the polyol method and reported high catalytic activity, reaction reversibility, peak current ratio, electron transfer rate constant, and excellent efficiencies for Pt-included catalysts. This result significantly improves the operational effectiveness of VRFB. Tsai et al.[156] used a synchronous technique to create Ir-modified graphene (Ir-G), which has a high affinity for oxygen species, effectively adsorbs VO^{2+}/VO_2^{+}[157], and exhibits modest peak potential difference and low oxidation potential, thereby promoting electrochemical activity and reversibility of the process, as well as the battery's energy storage efficiency[158]. In another investigation, Bi was combined with CNT to increase V^{2+}/V^{3+}reaction kinetics and inhibit hydrogen evolution on the negative side[159]. Blasi et al.[160] reported Ni-decorated CNF (Ni/CNF) as a catalyst for both VO^{2+}/VO_2^{+} and V^{2+}/V^{3+} redox processes. The carbothermal reduction of Ni species at high temperatures led to a more mesoporous structure and larger surface area than pure CNF. Additionally, Ni's graphitization catalysis on CNF increased

the conductivity of Ni/CNF[161]. Moreover, Ni/CNF has a larger concentration of C=O and C-O than CNF, which encourages vanadium adsorption and increases the material's electrocatalytic activity.

4.3 Carbon Paper

Table 4: Recent advances in CP as electrode material with different types of catalyst in VRFB.

Catalyst	**Deposition Method**	**Electrolytes**	**Current density ($mAcm^{-2}$)**	**VE (%)**	**CE (%)**	**EE (%)**	**Cycling Stability (Cycles)**	**Ref.**
Activated carbon (coconut shell)	Coating	1.7M V_2O_5 + 4M H_2SO_4	10	-	90	85	100	[162]
Turbostratic carbon	Coating	0.1M $VOSO_4$ + 2M H_2SO_4	10	96	87	84	200	[163]
Black pearl carbon	-	1.5M $VOSO_4$ + 2M H_2SO_4	35	77	92	96	800	[164]
TiC	Dip-coating	0.05M V-ion + 3M H_2SO_4	100	85		80.7	30	[165]
TiN-NPs	Drop-cast	1M $VOSO_4$ + 3M H_2SO_4	30	89.1	91.7	81.7	50	[166]
MnO_2	Redox deposition method	0.8M V-ion + 3M H_2SO_4	50	82.2	97	75.6	50	[167]
Cobalt oxide	Etching method	1.5M V-ion + 3M H_2SO_4	50	-	-	89	50	[168]
N-Carbon nanostructures	Chemical vapour deposition	1.5M $VOSO_4$ + 2M H_2SO_4	400	80	92	72	50	[169]
Bismuth-polyaniline	Thermally-treated	1.6M $VOSO_4$+ 3M H_2SO_4	80	-	-	68	200	[170]
Carbon allotropes	Prototypal deposition	-	600	-	-	70.8	-	[171]

Electrodes made of carbon paper (CP) are often employed in many electrochemical applications, such as flow batteries and fuel cells. Nevertheless, it has been shown that the kinetics of redox processes, such VO^{2+}/VO_2^{+} in VRFBs, are comparatively sluggish, leading to considerable activation losses during operation. This may be solved by effectively treating CP formed of carbon fibres with a solution of mixed acids. At longer treatment times, there are more -OH groups on the CP. However, highly hydroxylated CP may show the highest activity towards the redox reactions of V^{2+}/V^{3+} and V^{4+}/V^{5+} due to the serious damage to the surface. Table 4 summarizes previous

research studies that have used CP as an electrode material with various types of catalysts for VRFBs.

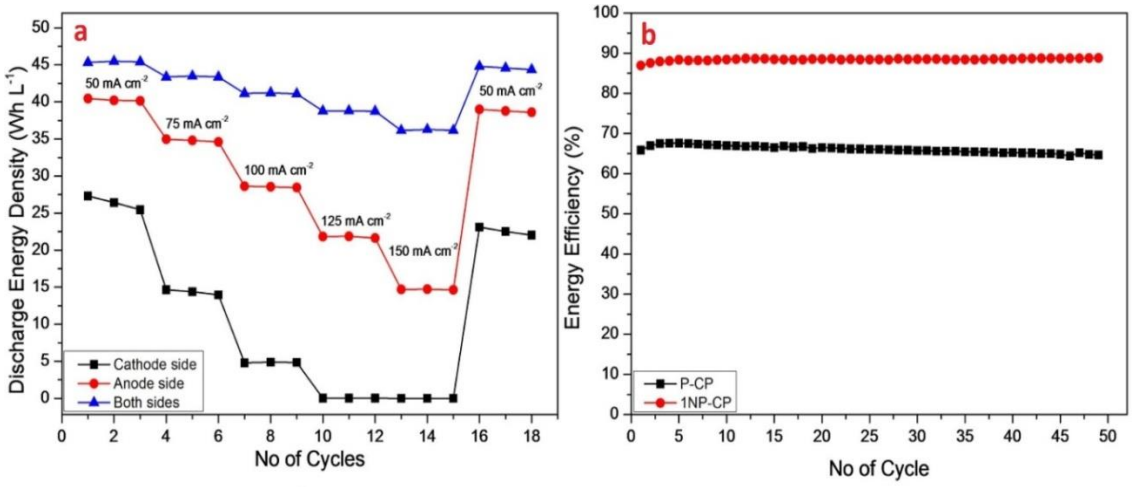

Figure 8: Discharge energy densities (a), EE (b) at 50 $mAcm^{-2}$ for P-CP, TT-CP or 1NP-CP. Reprinted from publication[168], Copyright (2022), with permission from Elsevier.

Abbas et al.[168] modified the CP electrode and found that the thin, nanoporous, and functionalized carbon paste demonstrated a synergistic effect resulting in increased electrolyte utilization (110%), discharge energy density (46 WhL^{-1}), and EE (29%) at a current density of 50 $mAcm^{-2}$, as shown in Figure 8. Other studies focused on modifying CP electrodes with additional materials, such as coconut shell-acquired high surface area mesoporous carbon by Ulaganathan et al.[162]. They believed that this modification could improve the VRFB's cell performance and lead to a considerable increase in energy density; V^{3+}/V^{4+} redox couple provides the additional electrons for the electrochemical reaction without influencing the conventional V^{4+}/V^{5+} couple. The presence of such a gain of electrons is mainly because of the utilization of high surface area mesoporous carbon and its superior electro-catalytic activity. Using processed industrial waste tyre carbon, Kumar et al.[163] created turbostratic carbon (TC), which has a surface area of 875 m^2g^{-1},

low charge transfer resistance, quick electron transfer process, high peak current, and low peak potential difference. The cell's performance remained stable for up to 200 cycles.

Bellani et al.[172] investigated the electrochemical performance of two graphitic carbon powders, MWCNTs and GNP, along with two mesoporous acetylene carbon blacks and Vulcan. The black pearl demonstrated low activation energy and peak separation values for both electrode reactions, which were lower than those reported for N-doped carbon black for anode and cathode reactions, and smaller than those reported by Han et al.[173] for V^{2+}/V^{3+} and V^{4+}/V^{5+} on GO nanoplatelets. Among the tested materials, black pearl exhibited the fastest kinetics for small potential peak separations on both electrodes, except for rGO reported by Li et al.[138]. However, the high cost of rGO due to the high energy required to synthesize it makes it uneconomical for large-scale use. In order to grow nitrogen-containing carbon nanostructures (N-CP) on commercial CP, Sodiq et al.[164] utilized CVD. This led to improved kinetics and durability of the electrode for V^{3+}/V^{2+}redox reactions as well as significant suppression of the peak potential separation ($\Delta E \sim 80$ mV), indicating faster kinetics than conventional CP ($\Delta E \sim 160$ mV).

In the metal-based category, Jiang et al.[167] utilized the redox deposition method to fabricate MnO_2 nanosheet array-decorated carbon paste without a binder as a negative electrode. The resulting electrode exhibited outstanding electrocatalytic performance and hydrophilicity, along with higher discharge capacity and better capacity retention (50 cycles at 50 $mAcm^{-2}$) compared to the pristine felt. The resulting energy efficiency (EE) was around 75.6% at 100 $mAcm^{-2}$, compared with 70.2% for the pristine cell. Meanwhile, Yang et al.[166] investigated TiN-coated CP, and their findings indicate that a single VRFB cell's CE, VE, and EE were 91.74%, 89.11%, and 81.74%, respectively, at a charge-discharge current density of 30 $mAcm^{-2}$. When tested with 50 charge-discharge cycles, the VRFB with TiN nanoparticles maintained CE values

consistently above 90%. Pahlevaninezhad et al[170] introduced carbonized bismuth-polyaniline on a thermally-treated CP and found EE 68% at 80 $mAcm^{-2}$.Fiorini et al[171] proposed prototypal deposition method of high-throughput carbon allotropes on CP and achieved EE 70.8% at 600 $mAcm^{-2}$.

The team of Wei et al.[165] developed a composite electrode by incorporating TiC nanoparticles onto CP to serve as the negative electrode in a single-cell VRFB. The TiC nanoparticles exhibit high catalytic activity, and as a result, the redox reaction of V^{3+}/V^{2+} in acid solution is significantly catalyzed. When compared to the potential of pure carbon nanoparticles and pristine CP, the oxidation peak potential is adversely displaced by 100 and 183 mV, respectively. The flow battery performance exhibited an EE of 80.7% at 100 $mAcm^{-2}$, which is 12.3% higher than the pristine electrode.

4.5 Summary

In conclusion, carbon-based, metal-based, and carbon-metal composite-based electrocatalysts have been frequently employed to modify GF, CF, and CP electrodes. However, because of their small active surface area and high concentration polarization, CP electrodes have not been widely employed. These electrodes have been doped with carbon- and metal-based electrocatalysts to enhance their electrochemical properties. It's have also undergone various processing and manufacturing steps to increase the number of functional groups, surface area, reversibility, and reaction kinetics. The use of both carbon-based and metal-based electrocatalysts through doping has resulted in increased EE, VE, CE, discharge capacity, and energy density. Noble metals have the potential to improve electrocatalytic activity and reduce the overall potential of GF electrodes, but these methods are not practical for large-scale applications due to their high cost, poor mechanical stability, sensitivity to unwanted oxygen and substantial hydrogen evolution side

reactions, and other factors. It was also found that while improvements in charge-discharge capacity and maximum current densities have been achieved, the electrocatalyst breakdown and agglomeration can limit their long-term performance.

5.0 POTENTIAL OF MXENES AS ELECTRODE ACTIVE MATERIAL IN VRFBs

5.1 Introduction

A novel family of 2D transition metal compounds called MXenes is created by chemically etching carbides, nitrides, or carbonitrides. These nanomaterials were first reported in 2011[174], with the first MXene (Ti_3C_2) (Figure 9 (b)) produced by selectively removing the Al layers from the Ti_3AlC_2 MAX phase precursor (Figure 9 (a)) using etchants. MXenes are part of a large family of 2D materials with the general formula $M_{n+1}X_nT_x$ (n=1-4), where M is a transition metal (Ti, V, Mn, Nb, Zr, Mo, Hf, Ta, Cr, Sc, W), X is a combination of C and/or N atoms, and T_x represents the surface terminations (-F, -O, -OH, -Cl, and -Br) of the outermost transition metal layers as depicted on Figure 9.

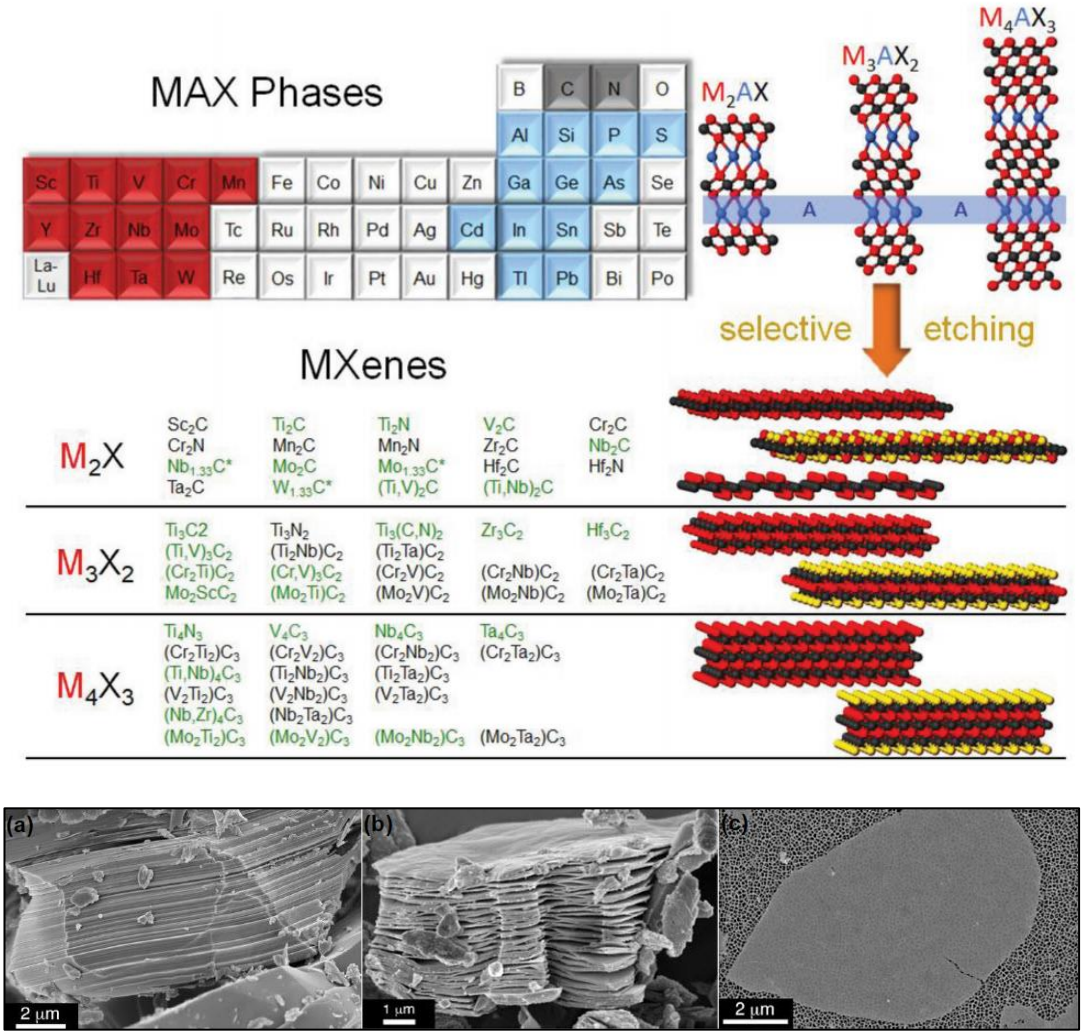

Figure 9: A variety of different configurations based on 12 transition metals (red), 12 groups of A elements (blue), and 2X elements (black) that result in M_2AX, M_3AX_2, or M_4AX_3 structures of MAX phase. Nearly 30 MXenes have been experimentally produced through selective etching of the A layer from MAX phases (marked in green) and the others are theoretically predicted (marked in black). MXenes are defined in chemical formulas of M_2X, M_3X_2, or M_4X_3. Reprinted with permission from[175], Copyright (2022), with permission from John Wiley and Sons. The FESEM images of the (a) MAX phase (Ti_3AlC_2), (b) MXenes (Ti_3C_2), and (c) Ti_3C_2 single layer are presented. Reprinted with permission from[176], Copyright (2022), American Chemical Society.

MXenes are typically produced using a top-down approach, involving chemical etching of the A-layer atoms (such as Al, Si, Ga) from MAX phases, which are ternary carbides, nitrides or carbonitrides of transition metals with layered hexagonal structures. The resulting loosely-stacked MXene layers can be further separated into single-layer (Figure 9(c)) or few-layer flakes via delamination (Figure 10). The advantages of MXenes and their potential applications as electrode materials for VRFBs will be discussed in the following section.

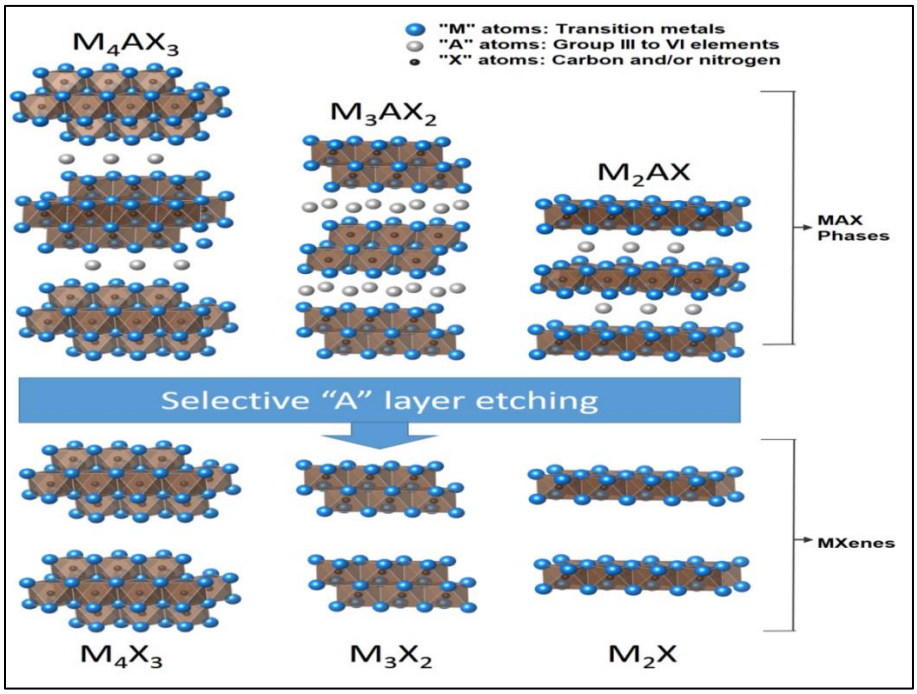

Figure 10: MAX phases are converted into MXenes via selective etching of layers consisting of A atoms of an element which originated from any of the groups IIIA to VIA.

5.2 Connecting MXenes' Properties and Features to Electrode Materials

Based on Figure 9, a wide range of transition metals in the M site can be utilized to form MXenes. The ability of MXenes to produce solid solutions and carbonitrides involving the M and X sites enables the creation of an almost limitless variety of 2D materials with varying structures. A solid solution consists of two different transition metals occupying the M sites in the MXene structure

randomly. Through selective etching of the A layer from MAX phases, nearly 30 distinct stoichiometric MXenes (marked in green in Figure 9) have been physically synthesized, and many more compositions have been theoretically explored through density functional theory (DFT) calculations[177]. During selective etching, newly exposed transition metal atoms (M) are instantly coordinated by anions (=O, -OH, or -F) from the etchant to form surface terminations T_x, which can be tailored for specific redox chemistries[178]. With various choices of transition metal atoms, solid solution formation, and diverse surface chemistry due to surface termination, MXenes offer vast opportunities to tailor and create MXenes with desirable and distinct properties in the realm of 2D nanomaterials.

MXenes stand out among other available 2D materials such as graphene, graphite, CNTs, silicone, germanium compounds, etc., due to their remarkable physical and chemical features, including a large variety of compositions, 2D structures, and surface and interlayer chemistries. Unlike other 2D materials, such as semiconductors, semimetals, and dielectrics, MXenes possess exceptional metallic electrical conductivity, with values reported up to 20,000 Scm^{-1} for Ti_3C_2[179], allowing them to be applied as current collectors, interconnects, and conductive fillers. Most MXenes behave similarly to metals in terms of electron transport, with resistivity decreasing linearly with temperature. The resistivity-temperature relation can be reversed and result in semiconductor-like behavior by changing the type of transition metal and the way the M site is built in MXenes. The surface termination can alter the density of states (DOS), and thus the Fermi levels are shifted and tuned, making MXenes electronically tunable[175]. However, the complexity of surface termination, including non-uniform termination, type and position of termination, or completely non-terminated MXenes, remains a challenge in the synthesis of these 2D materials, but it also offers a great opportunity to form desired MXenes since their electronic properties are

largely influenced by these aspects. Additionally, the electrical, mechanical, optical, thermal, and magnetic characteristics of MXenes can be significantly impacted by the surface terminations[180].

In VRFBs, the supply and storage of energy are regulated by the redox reaction of redox couples/pairs ($V^{2+}/V^{3+}$and VO^{2+}/VO_2^{+}) dissolved in the electrolytes. Both electrodes (anode and cathode) do not participate in the reaction, but they influence the performance of VRFBs by providing active sites for redox reactions. Their electrochemical activity affects the charge-discharge voltages and, as a result, the VE during the battery cycle operation. The electrode must exhibit electrochemical stability within the operating potential window of VRFB. To maximize the charge transfer rate linked with ohmic losses, cell voltage, and EE, the electrode must also have excellent electrical conductivity. The important requirements for electrode materials in VRFBs, which are high electrochemical activity, excellent electrical conductivity and large surface area, are fundamentally fulfilled by the MXenes. Since their invention, MXenes have been intensively explored for electrochemical energy storage in lithium-ion (Li^+) batteries and supercapacitors due to their electrical conductivity, high surface area, and redox capability[174a, 177]. However, there is a limited study of applying MXenes as electrode active material in VRFBs. In this case, the transition metal core layers of MXenes enable rapid electron transport via the electrode, enabling an ultrahigh charging rate, and surface termination of transition metal oxide provides a redox-active surface for pseudocapacitive charge storage, making MXenes unquestionably qualified[177]. MXenes are promising electrode materials because of the two aforementioned characteristics[181]. In addition, due to the ability to tune their chemical, structural, and surface chemistry, MXenes offer a wide range of working potentials, making them viable candidates for either anodes or cathodes[182].

The MXenes can be processed in an aqueous solution without any use of surfactants or binders as they are hydrophilic due to their nature of surface chemistry. They are sometimes called "electrically conductive clay" as their rheological characteristics are comparable to those of clay[183]. The hydrophilicity renders them having aqueous solution processability, which can be produced in scalable amounts (kg batches)[178] for a wide range of applications**,** which are essentially required by VRFBs. In addition, MXenes are potentially be used as electrodes thanks to redox-active transition metal atoms with surfaces terminated with -O or -OH.

Intercalation in MXenes is convenient mainly because of their layered structure[184].The composition of the MAX phase and the etchant being used could influence and manipulate the interlayer distance between individual flakes in MXene stacks. These two parameters influence the interlayer distance by influencing the number of surface functional groups and the potency of hydrogen bonds formed between MXene layers. Furthermore, MXenes offer further control of interlayer distance via intercalation capability, which can be achieved by using monomers, surfactants, cationic solvents, argon, N-doping, applied voltage, etc.[185]. Polar organic molecules[186] and metal ions (Li^+, Na^+, K^+, $NH_4^+$and Mg^{2+})[180] are capable of intercalating MXenes and occupying active sites on the MXene surfaces. With that, ion accessibility into the 2D structure is enhanced to improve electrochemical performance[184, 187].

In VRFBs, electrode materials must be chemically stable in a strongly acidic aqueous solution, based on the fact that the battery system utilises a strongly acidic aqueous solution as electrolytes for the redox couples. The stability of MXenes is strongly influenced by their inherent chemical composition and microstructure, which are closely related to their surface termination types and M layers. MXene nanosheets or films were shown to have poor chemical durability in water and ambient conditions in the most of previous studies. The reason for this is the

modification of the structure, which occurs as a result of the combined effects of air, moisture, and light, leading to the undesirable oxidation and degradation of the properties[188]. These types of deterioration may drastically degrade the structure's integrity, shortening its lifespan, thus making it unsuitable for future applications. Nonetheless, a homogenous surface encapsulation strategy can provide an additional barrier to ambient environments, hence increasing the MXenes' environmental stability[188]. Since oxidation mostly initiates at the edges of MXenes, it is possible to mitigate oxidation by passivating the edges with inert oxides or impermeable materials. Alternatively, optimising the size of MXene nanosheets with a bigger lateral size rather than a smaller one boosts not only their oxidation stability but also their activity for various applications[188].

While many MXenes have been synthesized, the majority of reported MXenes are carbides, and only a few types of MXenes, such as $Ti_3C_2T_x$ and Nb_2CT_x, have been studied for their oxidation performance. It is not yet well understood which MXenes are most stable under different conditions. Therefore, there is a need to explore other promising MXenes, such as $Nb_4C_3T_x$, and $Zr_3C_2T_x$, for use in severe conditions, such as high temperatures or acidic environments. Understanding the oxidation kinetics of MXenes is crucial to prevent or minimize oxidative degradation and encourage the utilization of MXenes as electrodes in VRFBs[188].

MXenes can be hybridized with other nanomaterials to create unique characteristics that cannot be provided by a single material. Catalytic and redox-active particles, organic molecules, 2D oxides, graphene, phosphorene, nanotubes, and conducting polymers have all been merged with MXenes[189]. For Li^+ batteries, porous MXene flakes were hybridized with CNTs to optimize the electrode structure, resulting in enhanced battery performance with a Li^+ capacity of over 750 $mAhg^{-1}$[174a]. MXene-based hybrid materials have better electrochemical performance, allowing

for improved ion accessibility in both aqueous and organic electrolytes, as well as improved ion movement within the electrodes[189b]. Therefore, the creation of heterostructures that consist of MXenes and other 2D materials or hybrid architectures may be utilized to generate battery electrodes that have improved capacity, high rate capabilities, and long cycle life[174a, 177, 189b].

5.3 Limited Research on MXenes for VRFBs

To date, CF, GF, and CP have been frequently utilized as electrode materials in VRFBs. These materials have high electrical conductivity, high porosity, and excellent chemical stability under harsh oxidizing conditions, which make them ideal candidates for VRFBs. However, they suffer from drawbacks such as low reaction kinetics, poor kinetic reversibility, inadequate wetting, and a small electrochemically active surface area[133a]. To enhance the electrochemical performance of VRFBs, internal modifications can be made, such as incorporating a nanostructured electrocatalyst with a large surface area and abundant surface groups[77].

Currently, carbon-based electrocatalyst has been a popular topic when discussing a suitable nanostructured catalyst and one of the more competent nanoparticle materials is the emerging 2D MXenes ($Ti_3C_2T_x$). The previous section noted that electrocatalysts made from MXenes possess desirable characteristics for use in VRFBs, such as high conductivity, hydrophilicity, surface area, and stability under anodic potentials[181]. Wei et al. demonstrated that MXene-modified graphite felt anodes with hollow titanium carbide nanoparticles as electrocatalysts achieved high energy efficiencies of 81.3% at 200 $mAcm^{-2}$ and 75.0% at 300 $mAcm^{-2}$, and showed good durability during cycling[190]. The improved performance was attributed to the increased surface area and enhanced kinetics resulting from nanoparticle modification.

The work on $Ti_3C_2T_x$ modified electrodes on anodic performance in VRFBs was done by Ali ValaMizrak et al. in 2021[181]. Adding MXene to CP electrodes can improve the

electrochemical performance of VRFBs. By lowering the activation overpotential, MXene-coated carbon paper electrodes made V^{2+}/V^{3+} redox reactions much more electrocatalytic. The hydrophobic CP's wetting was improved and active sites were generated, resulting in an increase in the electrochemically active surface area. Additionally, studies on charge-discharge cycles showed that $Ti_3C_2T_x$ batteries performed the best at all current densities tested. While MXene significantly catalyzed the anodic V^{2+}/V^{3+}redox pair, further investigation of the mass transport capacities of the electrodes in these electrochemical systems is necessary since high coating densities of porous electrodes make them prone to clogging.

5.4 Summary

MXenes have several unique properties that make them desirable for use as electrode materials in VRFBs. These include strong electrical conductivity, large surface areas, redox capabilities, adjustable surface chemistries, and solution processability due to their hydrophilicity. They are also available in a variety of compositions, interlayer spacing configurations, intercalation, and hybridization, making them even more attractive for use in VRFBs, in addition to their previous applications in energy storage and ultracapacitors. However, to avoid or minimize oxidation degradation, strategies must be employed to enhance their oxidation stability. Previous research has explored the use of MXenes as electrode materials in VRFBs, with observed improvements in electrochemical performance resulting from modifications in morphology and structure of MXenes.

6.0 CHALLENGES AND FUTURE DEVELOPMENTS

In electrochemical energy storage applications, interface compatibility and stability are crucial factors in designing effective electrodes. Customized interfaces are necessary to enable rapid and stable flux of ions and electrons, especially under high current and power densities, due to the various chemical and electrochemical potentials involved. The formation of a passivation layer at the boundary step between the charge carriers from the electrode is essential for stable battery activity over a large voltage window. To enhance the stability of electrode materials in harsh environments, it is beneficial to add a thin layer of coating, which can increase the structural strength of the materials, and a conformal passivating layer, which can reduce the interfacial impedance. Thin layers of passivation can reduce charge recombination at surface states, accelerate oxidation reaction kinetics, and protect the anode surface from chemical corrosion. It works as a functional layer. Passivation layers must have strong adhesion, even during straining, depending on the environment. They are usually chemically inert, corrosion-resistant dielectrics that operate as diffusion barriers to water diffusion and have a wide bandgap. Passivation layers are typically 100 nm thick, but more frequently 1 – 2 nm is employed to allow charges to transfer via tunneling. The cathode interfacial reactions can result in surface passivation, when the resulting conformal layers reach a critical thickness beyond which ordinarily maintained interfacial reactions stop. A direct cathode-gas chemical reaction, the passivation behavior is regulated by ionic water interaction driven ion de-intercalation. Furthermore, by reducing chemical delithiation, a thin disordered rocksalt layer generated on the cathode surface can effectively alleviate surface degradation[191]. The established passivation paradigm enables novel possibilities for the development of cathodes with high energy and stability. It enables easy ion migration, plating/stripping, and, despite the presence of a thicker layer, which indicates an initial greater electrolytes breakdown, a stable layer is finally produced, preventing future electrolytes reduction

of batteries. Van Genuchten et al.[192] increased the passivation overpotential and energy consumption in electrocoagulation, resulting in the formation of an anodic surface layer. Extreme passivation might generate electrochemical side reactions that reduce coagulant formation during galvanostatic operation or completely stop current flow during potentiostatic (constant voltage) operation[193]. However, investigating the ion and electron pathways and the electrochemical reactions in dynamic structures with flowing electrodes can be challenging, and more research is needed to fully understand how the interfacial structure and composition change over time and affect the overall electrochemical efficiency. However, there are still challenges in achieving optimal electrode performance in VRFBs, such as a limited operational potential range, stability issues, lower conductivity, low corrosion resistance, poor electrochemical activity, low specific area, high cost, and limited eco-friendliness, which require continued investigation.

To address the challenges faced by VRFB electrodes, several steps can be taken, such as introducing oxygen-containing functional groups through different electrode modification techniques to enhance reactivity and wettability during vanadium redox reactions. Additionally, developing an electrocatalyst on the electrode surface can improve specific surface area, stability, electrocatalytic properties, and electrical conductivity, reducing charge transfer resistance for better performance. Surface etching methods can also create high porous media, improving ion movement on the electrode surface. While carbon-based and metal-based electrocatalysts have shown good VRFB performance, composite carbon-metal electrocatalysts have demonstrated the best electrochemical and VRFB properties. To further optimize the electrocatalyst and synthesis route, studies on the morphology, modifying the crystal structure, and constructing heterojunction nanostructures are required. MXenes, with their unique 2D properties, high conductivity, large surface area, and redox capabilities, offer potential as electrode materials in VRFBs, but further

research is needed to improve their electrochemical activity and achieve superior physico-chemical performance.

The development of the VRFB electrode alone is not enough to ensure optimal performance; other components of the cell also require attention. In particular, improvements to cell stack design and electrolyte flow distribution are necessary to make VRFB systems more cost-effective. To achieve this, computational fluid dynamics simulations can be used to determine flow distribution and pressure drop in the VRFB system. These simulations can lead to better interaction between the electrolyte and electrode, as well as a more uniform distribution of electrolytes, which eliminates "dead zones" on the electrodes that may cause gas side reactions during charging. Another important factor affecting VRFB performance is the temperature of the electrolyte solution that affects the performance of VRFBs because it plays a significant role in the electrode reaction of vanadium ions. Optimum temperature can weaken the polarization concentration on the electrode surface and lead to more reversible reaction processes. It is necessary to reduce the polarization losses resulting from ohmic, concentration, and activation losses in order to enhance the performance of VRFBs.

7.0 CONCLUSIONS

VRFB is regarded as a highly prospective electrochemical setup for storing energy on a large scale. The VRFB electrode is a crucial component that significantly impacts the electrochemical activity and overall performance of VRFBs, including EE and power density. Currently, carbon-based electrodes such as GF, CF, and CP are commonly used. To enhance the performance of the electrode, two approaches are suggested: surface modification and the use of an electrocatalyst. Surface modification involves introducing oxygen-containing functional groups that can

potentially improve VRFB performance. Meanwhile, the development of ideal electrocatalyst materials requires specific properties such as a large active surface area, good electrical conductivity and chemical stability, and excellent electrochemical properties towards VO^{2+}/VO_2^{+} and V^{2+}/V^{3+} redox reactions. Additionally, 2D materials such as MXene are promising candidates for VRFB electrode materials, particularly for negative V^{2+}/V^{3+} redox reactions, due to their unique structure and surface chemistry, excellent mechanical stability, metallic conductivity, and low cost. However, challenges remain, including insufficient surface-active sites, poor kinetic reversibility, and low electrochemical activity. Therefore, further development is needed to improve overall VRFB performance.

ACKNOWLEDGEMENT

The authors wish to acknowledge the financial support provided by Universiti Putra Malaysia and Sunway University through the project codes GP-IPB/2020/9688702 and GRTIN-IGS-RCNMET[S]-16-2022. Additionally, the authors express their gratitude to Md Showkot Hossain from the Faculty of Electrical Engineering, Universiti Teknikal Malaysia Melaka, 76100 Melaka, Malaysia, for contributing to this study.

REFERENCES

[1] A. Clemente, R. Costa-Castelló, *Energies* **2020**, *13*, 4514.
[2] in *Vanadium Redox Flow Batteries (VRFB) Market, Vol. 2022*, Transparency Market Research, **2022**.
[3] aM. Skyllas-Kazacos, (Ed.: U. Limited), **1988**; bM. Skyllas-Kazacos, M. Rychcik, R. G. Robins, A. G. Fane, M. A. Green, *J. Electrochem. Soc.*, *133*, 1057-1058.
[4] P. C. Ghimire, A. Bhattarai, T. M. Lim, N. Wai, M. Skyllas-Kazacos, Q. Yan, *Batteries* **2021**, *7*, 53.
[5] aY. Kumar, G. P. Pandey, S. A. Hashmi, *J. Phys. Chem. C* **2012**, *116*, 26118-26127; bK. Lourenssen, J. Williams, F. Ahmadpour, R. Clemmer, S. Tasnim, *J. Energy Storage* **2019**,

25, 100844; cS. P. Ressel, Universitat Politecnica De Valencia (Spain), **2019**; dM. Skyllas-Kazacos, M. Chakrabarti, S. Hajimolana, F. Mjalli, M. Saleem, *J. Electrochem. Soc.* **2011**, *158*, R55.

[6] J. Choi, W.-K. Park, I.-W. Lee, in *2016 IEEE International Conference on Renewable Energy Research and Applications (ICRERA)*, IEEE, **2016**, pp. 903-906.

[7] A. Lucas, S. Chondrogiannis, *Int. J. Electrical Power & Energy Systems* **2016**, *80*, 26-36.

[8] T. Jirabovornwisut, A. Arpornwichanop, *Int. J. Hydrogen Energy* **2019**, *44*, 24485-24509.

[9] aK.-H. Shin, C.-S. Jin, J.-Y. So, S.-K. Park, D.-H. Kim, S.-H. Yeon, *J. Energy Storage* **2020**, *27*, 101066; bC. Tempelman, J. Jacobs, R. Balzer, V. Degirmenci, *J. Energy Storage* **2020**, *32*, 101754.

[10] C. Choi, S. Kim, R. Kim, Y. Choi, S. Kim, H.-y. Jung, J. H. Yang, H.-T. Kim, *Renewable and Sustainable Energy Rev.* **2017**, *69*, 263-274.

[11] F. Nadeem, S. S. Hussain, P. K. Tiwari, A. K. Goswami, T. S. Ustun, *IEEE Access* **2018**, *7*, 4555-4585.

[12] T. Struckmann, P. Kuhn, S. Ressel, *Electrochim. Acta* **2020**, *362*, 137174.

[13] aK. J. Kim, M.-S. Park, Y.-J. Kim, J. H. Kim, S. X. Dou, M. Skyllas-Kazacos, *J. Mater. Chem. A* **2015**, *3*, 16913-16933; bH. Zhang, X. Li, J. Zhang, *Redox flow batteries: Fundamentals and applications*, CRC Press, **2017**.

[14] Y. Shi, C. Eze, B. Xiong, W. He, H. Zhang, T. Lim, A. Ukil, J. Zhao, *Appl. Energy* **2019**, *238*, 202-224.

[15] aN. Kausar, A. Mousa, M. Skyllas-Kazacos, *ChemElectroChem* **2016**, *3*, 276-282; bS. Peng, N. Wang, C. Gao, Y. Lei, X. Liang, S. Liu, Y. Liu, *Int. J. Electrochem. Sci* **2012**, *7*, 4314-4321; cR. Schweiss, A. Pritzl, C. Meiser, *J. Electrochem. Soc.* **2016**, *163*, A2089-A2094.

[16] aZ. Jiang, K. Klyukin, V. Alexandrov, *J. Chem. Phys.* **2016**, *145*; bM. Kazacos, M. Cheng, M. Skyllas-Kazacos, *J. Appl. Electrochem.* **1990**, *20*, 463-467.

[17] D. P. Dubal, P. Gomez-Romero, *2D Materials* **2016**, *3*, 031004.

[18] Y. Ahn, D. Kim, *J. Ind. Eng. Chem.* **2022**.

[19] J. Shan, D. Xiao, *Int. J. Green Energy* **2021**.

[20] Y. Quan, G. Wang, A. Li, X. Wei, F. Li, J. Zhang, J. Chen, R. Wang, *RSC Adv.* **2019**, *9*, 3838-3846.

[21] Y. Ji, Z. Y. Tay, S. F. Y. Li, *J. Membr. Sci.* **2017**, *539*, 197-205.

[22] Y. Ahn, D. Kim, *J. Ind. Eng. Chem.* **2019**, *71*, 361-368.

[23] Y. Ahn, D. Kim, *Energy Storage Mater.* **2020**, *31*, 105-114.

[24] L. Hao, Y. Wang, Y. He, *J. Electrochem. Soc.* **2019**, *166*, A1310-A1322.

[25] R. Xie, P. Ning, G. Qu, J. Li, M. Ren, C. Du, H. Gao, Z. Li, *Chem. Eng. J.* **2018**, *341*, 298-307.

[26] L. Yan, D. Li, S. Li, Z. Xu, J. Dong, W. Jing, W. Xing, *ACS Appl. Mater. Interfaces* **2016**, *8*, 35289-35297.

[27] aR. Gundlapalli, S. Jayanti, *J. Energy Storage* **2021**, *33*, 102078; bD. Reynard, H. Vrubel, C. R. Dennison, A. Battistel, H. Girault, *ChemSusChem* **2019**, *12*, 1222-1228.

[28] H. Chen, S. Wang, H. Gao, X. Feng, C. Yan, A. Tang, *J. Power Sources* **2019**, *427*, 154-164.

[29] aK. Ma, Y. Zhang, L. Liu, J. Xi, X. Qiu, T. Guan, Y. He, *Nat. Commun.* **2019**, *10*, 1-11; bD. Reed, E. Thomsen, B. Li, W. Wang, Z. Nie, B. Koeppel, V. Sprenkle, *J. Power Sources* **2016**, *306*, 24-31.

[30] aA. Khazaeli, A. Vatani, N. Tahouni, M. H. Panjeshahi, *J. Power Sources* **2015**, *293*, 599-612; bX. Ma, H. Zhang, C. Sun, Y. Zou, T. Zhang, *J. Power Sources* **2012**, *203*, 153-158.
[31] J. Piwek, C. Dennison, E. Frackowiak, H. Girault, A. Battistel, *J. Power Sources* **2019**, *439*, 227075.
[32] J. Balaji, M. G. Sethuraman, S.-H. Roh, H.-Y. Jung, *Polym. Test.* **2020**, *89*, 106567.
[33] W. Li, R. Zaffou, C. C. Sholvin, M. L. Perry, Y. She, *ECS Trans.* **2013**, *53*, 93-99.
[34] B. G. Thiam, S. Vaudreuil, *J. Electrochem. Soc.* **2021**.
[35] in *Market Research Report, Vol. 2022*, DataIntelo, **2022**.
[36] Z. Šimić, D. Topić, G. Knežević, D. Pelin, *Int. J. Electrical Comp. Eng. Systems* **2021**, *12*, 53-65.
[37] B. Turker, S. A. Klein, L. Komsiyska, J. J. Trujillo, L. von Bremen, M. Kühn, M. Busse, *Energy Conv. Manage.* **2013**, *76*, 1150-1157.
[38] Á. Cunha, J. Martins, N. Rodrigues, F. Brito, *Int. J. Energy Res.* **2015**, *39*, 889-918.
[39] T. Shibata, S. Hayashi, T. Sano, K. Fujikawa, K. Yamanishi, Y. Tsutsui, in *Int. Flow Battery Forum. Limited Swanbarton*, **2017**, pp. 68-69.
[40] Z. Abdin, K. R. Khalilpour, in *Polygeneration with polystorage for chemical and energy hubs*, Elsevier, **2019**, pp. 77-131.
[41] in *Vanadium Redox Flow Battery (VRFB) Market, Vol. 2022*, Reports and Data, New York City, United States, **2022**.
[42] Z. Huang, A. Mu, *Int. J. Energy Res.* **2021**, *45*, 14170-14193.
[43] A. Chmielewski, J. Kupecki, Ł. Szabłowski, K. Fijałkowski, J. Zawieska, K. Bogdziński, O. Kulik, T. Adamczewski, *WWF Poland* **2020**.
[44] Z. Huang, A. Mu, L. Wu, H. Wang, *J. Energy Storage* **2021**, 103526.
[45] aK. Amini, J. Gostick, M. D. Pritzker, *Adv. Funct. Mater.* **2020**, *30*; bZ. Liu, Y. Zou, in *Redox Flow Batteries*, CRC Press, **2017**, pp. 77-125; cR. Wang, Y. Li, *Energy Storage Mater.* **2020**, *31*, 230-251.
[46] Y. Xiang, W. A. Daoud, *Electrochim. Acta* **2018**, *290*, 176-184.
[47] S. Kim, *Energy Storage Dev.* **2019**, 1-19.
[48] Y. Xie, Y. Zhou, *J. Mater. Res.* **2019**, *34*, 2472-2481.
[49] Y. Liu, Y. Shen, L. Yu, L. Liu, F. Liang, X. Qiu, J. Xi, *Nano Energy* **2018**, *43*, 55-62.
[50] W. Li, Z. Zhang, Y. Tang, H. Bian, T. W. Ng, W. Zhang, C. S. Lee, *Adv. Sci.* **2016**, *3*, 1500276.
[51] aG. F. Dewald, S. Ohno, M. A. Kraft, R. Koerver, P. Till, N. M. Vargas-Barbosa, J. Janek, W. G. Zeier, *Chem. Mater.* **2019**, *31*, 8328-8337; bB. K. Saikia, S. M. Benoy, M. Bora, J. Tamuly, M. Pandey, D. Bhattacharya, *Fuel* **2020**, *282*, 118796.
[52] aA. W. Bayeh, D. M. Kabtamu, Y.-C. Chang, T. H. Wondimu, H.-C. Huang, C.-H. Wang, *Sustain. Energy Fuels* **2021**, *5*, 1668-1707; bJ. Su, Z. Li, L. Hao, L. Qin, *Appl. Sci.* **2022**, *12*, 2304.
[53] aP. C. Ghimire, R. Schweiss, G. G. Scherer, N. Wai, T. M. Lim, A. Bhattarai, T. D. Nguyen, Q. Yan, *J. Mater. Chem. A* **2018**, *6*, 6625-6632; bM. Maleki, G. A. El-Nagar, D. Bernsmeier, J. Schneider, C. Roth, *Sci. Rep.* **2020**, *10*, 1-14.
[54] Y. Lv, C. Han, Y. Zhu, T. Zhang, S. Yao, Z. He, L. Dai, L. Wang, *J. Mater. Sci. Technol.* **2021**, *75*, 96-109.
[55] L. Wu, Y. Shen, L. Yu, J. Xi, X. Qiu, *Nano Energy* **2016**, *28*, 19-28.
[56] S. Kwon, Y. Suharto, K. J. Kim, *J. Ind. Eng. Chem.* **2021**, *98*, 231-236.
[57] L. Yu, F. Lin, L. Xu, J. Xi, *J. Energy Chem.* **2019**, *35*, 55-59.

[58] C. Zhao, Y. Li, Z. He, Y. Jiang, L. Li, F. Jiang, H. Zhou, J. Zhu, W. Meng, L. Wang, *J. Energy Chem.* **2019**, *29*, 103-110.
[59] Q. Li, Q. Dong, T. Zhang, Z. Xue, J. Li, Z. Wang, H. Sun, *Electrochim. Acta* **2022**, 139970.
[60] P. Mazúr, J. Mrlik, J. Pocedic, J. Vrána, J. Dundálek, J. Kosek, T. Bystron, *J. Power Sources* **2019**, *414*, 354-365.
[61] D. Aaron, S. Yeom, K. D. Kihm, Y. A. Gandomi, T. Ertugrul, M. M. Mench, *J. Power Sources* **2017**, *366*, 241-248.
[62] X. Zhang, D. Zhang, Z. Xu, K. Zhang, Y. Zhang, M. Jing, L. Liu, Z. Zhang, N. Pu, J. Liu, *Chem. Eng. J.* **2022**, *439*, 135718.
[63] G. Wei, M. Jing, X. Fan, J. Liu, C. Yan, *J. Power Sources* **2015**, *287*, 81-86.
[64] X. Zhou, Y. Zeng, X. Zhu, L. Wei, T. Zhao, *J. Power Sources* **2016**, *325*, 329-336.
[65] J.-M. Jeong, K. I. Jeong, J. H. Oh, Y. S. Chung, S. S. Kim, *Appl. Mater. Today* **2021**, *24*, 101139.
[66] S. Mehboob, G. Ali, H.-J. Shin, J. Hwang, S. Abbas, K. Y. Chung, H. Y. Ha, *Appl. Energy* **2018**, *229*, 910-921.
[67] H. Jiang, W. Shyy, Y. Ren, R. Zhang, T. Zhao, *Appl. Energy* **2019**, *233*, 544-553.
[68] G. Wei, C. Jia, J. Liu, C. Yan, *J. Power Sources* **2012**, *220*, 185-192.
[69] M. M. Loghavi, M. Zarei-Jelyani, Z. Niknam, M. Babaiee, R. Eqra, *J. Electroanal. Chem.* **2022**, *908*, 116090.
[70] Z. He, M. Li, Y. Li, L. Wang, J. Zhu, W. Meng, C. Li, H. Zhou, L. Dai, *Appl. Surf. Sci.* **2019**, *469*, 423-430.
[71] L. Xia, Q. Zhang, C. Wu, Y. Liu, M. Ding, J. Ye, Y. Cheng, C. Jia, *Surf. Coat. Technol.* **2019**, *358*, 153-158.
[72] M. Raja, H. Khan, S. Sankarasubramanian, D. Sonawat, V. Ramani, K. Ramanujam, *Catal. Today* **2021**, *370*, 181-188.
[73] L. Wei, T. Zhao, G. Zhao, L. An, L. Zeng, *Appl. Energy* **2016**, *176*, 74-79.
[74] L. Wei, T. Zhao, L. Zeng, X. Zhou, Y. Zeng, *Appl. Energy* **2016**, *180*, 386-391.
[75] W. Lee, C. Jo, S. Youk, H. Y. Shin, J. Lee, Y. Chung, Y. Kwon, *Appl. Surf. Sci.* **2018**, *429*, 187-195.
[76] D. O. Opar, R. Nankya, C. J. Raj, H. Jung, *Appl. Mater. Today* **2021**, *22*, 100950.
[77] L. Wei, T. Zhao, L. Zeng, Y. Zeng, H. Jiang, *J. Power Sources* **2017**, *341*, 318-326.
[78] X. Zhou, T. Zhao, Y. Zeng, L. An, L. Wei, *J. Power Sources* **2016**, *329*, 247-254.
[79] D. M. Kabtamu, J.-Y. Chen, Y.-C. Chang, C.-H. Wang, *J. Power Sources* **2017**, *341*, 270-279.
[80] Y. Lv, J. Zhang, Z. Lv, C. Wu, Y. Liu, H. Wang, S. Lu, Y. Xiang, *Electrochim. Acta* **2017**, *253*, 78-84.
[81] M. Jing, X. Qi, X. An, X. Ma, D. Fang, X. Fan, J. Liu, C. Yan, *Electrochim. Acta* **2021**, *390*, 138879.
[82] A. Fetyan, G. A. El-Nagar, I. Derr, P. Kubella, H. Dau, C. Roth, *Electrochim. Acta* **2018**, *268*, 59-65.
[83] Z. He, L. Dai, S. Liu, L. Wang, C. Li, *Electrochim. Acta* **2015**, *176*, 1434-1440.
[84] J. Sun, M. Wu, X. Fan, Y. Wan, C. Chao, T. Zhao, *Energy Storage Mater.* **2021**, *43*, 30-41.
[85] M. Jing, X. Zhang, X. Fan, L. Zhao, J. Liu, C. Yan, *Electrochim. Acta* **2016**, *215*, 57-65.
[86] Z. He, M. Li, Y. Li, C. Li, Z. Yi, J. Zhu, L. Dai, W. Meng, H. Zhou, L. Wang, *Electrochim. Acta* **2019**, *309*, 166-176.

[87] Z. He, M. Li, Y. Li, J. Zhu, Y. Jiang, W. Meng, H. Zhou, L. Wang, L. Dai, *Electrochim. Acta* **2018**, *281*, 601-610.
[88] M.-A. Goulet, A. Habisch, E. Kjeang, *Electrochim. Acta* **2016**, *206*, 36-44.
[89] Y. Suharto, K. Lee, K. J. Kim, *J. Ind. Eng. Chem.* **2019**, *70*, 290-298.
[90] J. Li, X. Li, E. El Sawy, S. Maslovara, N. Yasri, V. Birss, E. P. Roberts, *Available at SSRN 4369447*.
[91] Y. Zhang, X. Zhang, Z. Xu, D. Zhang, W. Yu, Y. Zhang, L. Liu, J. Liu, C. Yan, *J. Power Sources* **2022**, *552*, 232241.
[92] Y. Liu, Y. Jiang, Y. Lv, Z. He, L. Dai, L. Wang, *Molecules* **2021**, *26*, 5085.
[93] Y.-T. Ou, D. M. Kabtamu, A. W. Bayeh, H.-H. Ku, Y.-L. Kuo, Y.-M. Wang, N.-Y. Hsu, T.-C. Chiang, H.-C. Huang, C.-H. Wang, *Catalysts* **2021**, *11*, 1188.
[94] R. Madhu, F. V. Kusmartsev, K.-h. Kim, H.-J. Ahn, *Electrochim. Acta* **2023**, *439*, 141619.
[95] V. Mahanta, M. Raja, R. Kothandaraman, *Mater. Lett.* **2019**, *247*, 63-66.
[96] C. Noh, B. W. Kwon, Y. Chung, Y. Kwon, *J. Power Sources* **2018**, *406*, 26-34.
[97] Q. Li, A. Bai, Z. Qu, T. Zhang, J. Li, X. Zhang, M. Yu, Z. Xue, H. Sun, *J. Chem.* **2019**, *2019*.
[98] S. Jeong, S. An, J. Jeong, J. Lee, Y. Kwon, *J. Power Sources* **2015**, *278*, 245-254.
[99] D.-S. Yang, J. Y. Lee, S.-W. Jo, S. J. Yoon, T.-H. Kim, Y. T. Hong, *Int. J. Hydrogen Energy* **2018**, *43*, 1516-1522.
[100] Q. Ma, Q. Deng, H. Sheng, W. Ling, H.-R. Wang, H.-W. Jiao, X.-W. Wu, W.-X. Zhou, X.-X. Zeng, Y.-X. Yin, *Sci. China Chem.* **2018**, *61*, 732-738.
[101] D. Cheng, G. Cheng, Z. He, L. Dai, L. Wang, *Int. J. Energy Res.* **2019**, *43*, 4473-4482.
[102] A. W. Bayeh, D. M. Kabtamu, Y. C. Chang, G. C. Chen, H. Y. Chen, G. Y. Lin, T. R. Liu, T. H. Wondimu, K. C. Wang, C. H. Wang, *ACS Sustain. Chem. Eng.* **2018**, *6*, 3019-3028.
[103] X. Wu, H. Xu, L. Lu, H. Zhao, J. Fu, Y. Shen, P. Xu, Y. Dong, *J. Power Sources* **2014**, *250*, 274-278.
[104] H. Zhou, J. Xi, Z. Li, Z. Zhang, L. Yu, L. Liu, X. Qiu, L. Chen, *RSC Adv.* **2014**, *4*, 61912-61918.
[105] B. Li, M. Gu, Z. Nie, X. Wei, C. Wang, V. Sprenkle, W. Wang, *Nano Lett.* **2014**, *14*, 158-165.
[106] Y. Shen, H. Xu, P. Xu, X. Wu, Y. Dong, L. Lu, *Electrochim. Acta* **2014**, *132*, 37-41.
[107] H. Zhou, Y. Shen, J. Xi, X. Qiu, L. Chen, *ACS Appl. Mater. Interfaces* **2016**, *8*, 15369-15378.
[108] D. M. Kabtamu, Y.-C. Chang, G.-Y. Lin, A. W. Bayeh, J.-Y. Chen, T. H. Wondimu, C.-H. Wang, *Sustain. Energy Fuels* **2017**, *1*, 2091-2100.
[109] A. W. Bayeh, D. M. Kabtamu, Y.-C. Chang, G.-C. Chen, H.-Y. Chen, G.-Y. Lin, T.-R. Liu, T. H. Wondimu, K.-C. Wang, C.-H. Wang, *J. Mater. Chem. A* **2018**, *6*, 13908-13917.
[110] Y. Ji, J. L. Li, S. F. Y. Li, *J. Mater. Chem. A* **2017**, *5*, 15154-15166.
[111] W.-F. Liu, K.-H. Kim, H.-J. Ahn, *J. Alloys Compounds* **2023**, 170106.
[112] S. Mohan, M. Revanasiddappa, M. Vellakkat, *Synthetic Metals* **2023**, *294*, 117311.
[113] J.-Y. Uan, Y.-J. Chen, Y.-H. Hsu, A. Arpornwichanop, Y.-S. Chen, *Mater. Today Commun.* **2021**, *27*, 102280.
[114] Z. He, L. Shi, J. Shen, Z. He, S. Liu, *Int. J. Energy Res.* **2015**, *39*, 709-716.
[115] Y.-H. Wang, I.-M. Hung, C.-Y. Wu, *Ceramics Int.* **2018**, *44*, S30-S33.
[116] J. Ortiz-Medina, Z. Wang, R. Cruz-Silva, A. Morelos-Gomez, F. Wang, X. Yao, M. Terrones, M. Endo, *Adv. Mater.* **2019**, *31*.

[117] Z. He, Y. Jiang, H. Zhou, G. Cheng, W. Meng, L. Wang, L. Dai, *Int. J. Energy Res.* **2017**, *41*, 439-447.
[118] Y.-C. Chang, J.-Y. Chen, D. M. Kabtamu, G.-Y. Lin, N.-Y. Hsu, Y.-S. Chou, H.-J. Wei, C.-H. Wang, *J. Power Sources* **2017**, *364*, 1-8.
[119] R. K. Gautam, A. Verma, *Mater. Chem. Phys. Rep.* **2020**, *251*, 123178.
[120] A. Hassan, T. Tzedakis, *J. Energy Storage* **2019**, *26*, 100967.
[121] L. Dai, Y. Jiang, W. Meng, H. Zhou, L. Wang, Z. He, *Appl. Surf. Sci.* **2017**, *401*, 106-113.
[122] Z. González, C. Flox, C. Blanco, M. Granda, J. R. Morante, R. Menéndez, R. Santamaría, *J. Power Sources* **2017**, *338*, 155-162.
[123] S. Fu, C. Zhu, Y. Zhou, G. Yang, J.-W. Jeon, J. Lemmon, D. Du, S. K. Nune, Y. Lin, *Electrochim. Acta* **2015**, *178*, 287-293.
[124] J. Jin, X. Fu, Q. Liu, Y. Liu, Z. Wei, K. Niu, J. Zhang, *ACS Nano* **2013**, *7*, 4764-4773.
[125] L. Shi, S. Liu, Z. He, J. Shen, *Electrochim. Acta* **2014**, *138*, 93-100.
[126] V. Pasala, J. N. Ramavath, C. He, V. K. Ramani, K. Ramanujam, *ChemistrySelect* **2018**, *3*, 8678-8687.
[127] H. Gursu, M. Gencten, Y. Sahin, *Int J Electrochem Sci* **2018**, *13*, 875-885.
[128] D. M. Kabtamu, J.-Y. Chen, Y.-C. Chang, C.-H. Wang, *J. Mater. Chem. A* **2016**, *4*, 11472-11480.
[129] D. M. Kabtamu, A. W. Bayeh, T.-C. Chiang, Y.-C. Chang, G.-Y. Lin, T. H. Wondimu, S.-K. Su, C.-H. Wang, *Appl. Surf. Sci.* **2018**, *462*, 73-80.
[130] Z. González, A. Sánchez, C. Blanco, M. Granda, R. Menéndez, R. Santamaría, *Electrochem. Commun.* **2011**, *13*, 1379-1382.
[131] H. Jiang, W. Shyy, M. Wu, L. Wei, T. Zhao, *J. Power Sources* **2017**, *365*, 34-42.
[132] W. Wang, X. Wang, *Electrochim. Acta* **2007**, *52*, 6755-6762.
[133] aJ. Xu, Y. Zhang, Z. Huang, C. Jia, S. Wang, *Energy and Fuels* **2021**, *35*, 8617-8633; bL. Zeng, T. S. Zhao, L. Wei, Y. K. Zeng, X. L. Zhou, *Energy Technol.* **2018**, *6*, 1228-1236.
[134] J. Jiang, Y. Zhang, P. Nie, G. Xu, M. Shi, J. Wang, Y. Wu, R. Fu, H. Dou, X. Zhang, *Adv. Sustain. Systems* **2018**, *2*.
[135] R. K. Sankaralingam, S. Seshadri, J. Sunarso, A. I. Bhatt, A. Kapoor, *J. Energy Storage* **2021**, *41*, 102857.
[136] M. Park, J. Ryu, Y. Kim, J. Cho, *Energy Environ. Sci.* **2014**, *7*, 3727-3735.
[137] W. Li, J. Liu, C. Yan, *Carbon* **2011**, *49*, 3463-3470.
[138] W. Li, J. Liu, C. Yan, *Carbon* **2013**, *55*, 313-320.
[139] M. Park, I.-Y. Jeon, J. Ryu, H. Jang, J.-B. Back, J. Cho, *Nano Energy* **2016**, *26*, 233-240.
[140] M. Park, Y. J. Jung, J. Kim, H. I. Lee, J. Cho, *Nano Lett.* **2013**, *13*, 4833-4839.
[141] K. J. Kim, M.-S. Park, J.-H. Kim, U. Hwang, N. J. Lee, G. Jeong, Y.-J. Kim, *Chem. Commun.* **2012**, *48*, 5455-5457.
[142] S. Jeong, S. Kim, Y. Kwon, *Electrochim. Acta* **2013**, *114*, 439-447.
[143] T.-M. Tseng, R.-H. Huang, C.-Y. Huang, C.-C. Liu, K.-L. Hsueh, F.-S. Shieu, *J. Electrochem. Soc.* **2014**, *161*, A1132-A1138.
[144] G. Wei, X. Fan, J. Liu, C. Yan, *J. Power Sources* **2015**, *281*, 1-6.
[145] S. E. Park, S. Y. Yang, K. J. Kim, *Appl. Surf. Sci.* **2021**, *546*, 148941.
[146] Z. Hu, Z. Miao, Z. Xu, X. Zhu, F. Zhong, M. Ding, J. Wang, X. Xie, C. Jia, J. Liu, *Chem. Eng. J.* **2022**, *450*, 138377.
[147] Y. Lv, Y. Yang, J. Gao, J. Li, W. Zhu, L. Dai, Y. Liu, L. Wang, Z. He, *Electrochim. Acta* **2022**, *431*, 141135.

[148] Y. Shao, X. Wang, M. Engelhard, C. Wang, S. Dai, J. Liu, Z. Yang, Y. Lin, *J. Power Sources* **2010**, *195*, 4375-4379.
[149] H. Lee, H. Kim, *J. Appl. Electrochem.* **2013**, *43*, 553-557.
[150] M. E. Lee, H.-J. Jin, Y. S. Yun, *RSC Adv.* **2017**, *7*, 43227-43232.
[151] M. Han, H. Kim, *J. Korean Electrochem. Soc.* **2018**, *21*, 1-5.
[152] Z. González, C. Botas, C. Blanco, R. Santamaría, M. Granda, P. Álvarez, R. Menéndez, *Nano Energy* **2013**, *2*, 1322-1328.
[153] M. Park, I. Y. Jeon, J. Ryu, J. B. Baek, J. Cho, *Adv. Energy Mater.* **2015**, *5*.
[154] B. Sun, M. Skyllas-Kazakos, *Electrochim. Acta* **1991**, *36*, 513-517.
[155] M. G. Hosseini, S. Mousavihashemi, S. Murcia-López, C. Flox, T. Andreu, J. R. Morante, *Carbon* **2018**, *136*, 444-453.
[156] H.-M. Tsai, S.-J. Yang, C.-C. M. Ma, X. Xie, *Electrochim. Acta* **2012**, *77*, 232-236.
[157] C. Chang, T. Yuen, Y. Nagao, H. Yugami, *J. Power Sources* **2010**, *195*, 5938-5941.
[158] C. P. De Leon, A. Frías-Ferrer, J. González-García, D. Szánto, F. C. Walsh, *J. Power Sources* **2006**, *160*, 716-732.
[159] S. Moon, B. W. Kwon, Y. Chung, Y. Kwon, *J. Electrochem. Soc.* **2019**, *166*, A2602-A2609.
[160] A. D. Blasi, C. Busacca, O. D. Blasi, N. Briguglio, V. Antonucci, *J. Electrochem. Soc.* **2018**, *165*, A1478-A1485.
[161] D. Cheng, Y. Li, J. Zhang, M. Tian, B. Wang, Z. He, L. Dai, L. Wang, *Carbon* **2020**, *170*, 527-542.
[162] M. Ulaganathan, A. Jain, V. Aravindan, S. Jayaraman, W. C. Ling, T. M. Lim, M. P. Srinivasan, Q. Yan, S. Madhavi, *J. Power Sources* **2015**, *274*, 846-850.
[163] R. Kumar, T. Bhuvana, A. Sharma, *ACS Sustain. Chem. Eng.* **2018**, *6*, 8238-8246.
[164] A. Sodiq, L. Mohapatra, F. Fasmin, S. Mariyam, M. Arunachalam, A. Kheireddine, R. Zaffou, B. Merzougui, *Chem. Commun.* **2019**, *55*, 10249-10252.
[165] L. Wei, T. Zhao, L. Zeng, X. Zhou, Y. Zeng, *Energy Technol.* **2016**, *4*, 990-996.
[166] C. Yang, H. Wang, S. Lu, C. Wu, Y. Liu, Q. Tan, D. Liang, Y. Xiang, *Electrochim. Acta* **2015**, *182*, 834-840.
[167] Y. Jiang, X. Feng, G. Cheng, Y. Li, C. Li, Z. He, J. Zhu, W. Meng, H. Zhou, L. Dai, *Electrochim. Acta* **2019**, *322*, 134754.
[168] S. Abbas, S. Mehboob, H.-J. Shin, O. H. Han, H. Y. Ha, *Chem. Eng. J.* **2019**, *378*, 122190.
[169] A. Sodiq, F. Fasmin, L. Mohapatra, S. Mariyam, M. Arunachalam, H. Hamoudi, R. Zaffou, B. Merzougui, *Mater. Adv.* **2020**, *1*, 2033-2042.
[170] M. Pahlevaninezhad, D. Momodu, M. Pahlevani, E. P. Roberts, in *Electrochem. Soc. Meeting Abstracts 241*, The Electrochemical Society, Inc., **2022**, pp. 493-493.
[171] S. Fiorini Granieri, G. M. Pagano, M. Messaggi, M. Zago, A. Casalegno, F. Di Fonzo, in *Electrochem. Soc. Meeting Abstracts 241*, The Electrochemical Society, Inc., **2022**, pp. 2036-2036.
[172] S. Bellani, L. Najafi, M. Prato, R. Oropesa-Nuñez, B. Martín-Garciá, L. Gagliani, E. Mantero, L. Marasco, G. Bianca, M. I. Zappia, C. Demirci, S. Olivotto, G. Mariucci, V. Pellegrini, M. Schiavetti, F. Bonaccorso, *Chem. Mater.* **2021**, *33*, 4106-4121.
[173] P. Han, H. Wang, Z. Liu, X. Chen, W. Ma, J. Yao, Y. Zhu, G. Cui, *Carbon* **2011**, *49*, 693-700.

[174] aB. Anasori, M. R. Lukatskaya, Y. Gogotsi, *Nat. Rev. Mater.* **2017**, *2*, 16098; bM. Naguib, M. Kurtoglu, V. Presser, J. Lu, J. Niu, M. Heon, L. Hultman, Y. Gogotsi, M. W. Barsoum, *Adv. Mater.* **2011**, *23*, 4248-4253.
[175] K. Hantanasirisakul, Y. Gogotsi, *Adv. Mater.* **2018**, *30*, 1804779.
[176] C. E. Shuck, M. Han, K. Maleski, K. Hantanasirisakul, S. J. Kim, J. Choi, W. E. Reil, Y. Gogotsi, *ACS Appl. Nano Mater.* **2019**, *2*, 3368-3376.
[177] A. VahidMohammadi, J. Rosen, Y. Gogotsi, *Science* **2021**, *372*, eabf1581.
[178] C. E. Shuck, A. Sarycheva, M. Anayee, A. Levitt, Y. Zhu, S. Uzun, V. Balitskiy, V. Zahorodna, O. Gogotsi, Y. Gogotsi, *Adv. Eng. Mater.* **2020**, *22*, 1901241.
[179] T. S. Mathis, K. Maleski, A. Goad, A. Sarycheva, M. Anayee, A. C. Foucher, K. Hantanasirisakul, C. E. Shuck, E. A. Stach, Y. Gogotsi, *ACS Nano* **2021**, *15*, 6420-6429.
[180] J. L. Hart, K. Hantanasirisakul, A. C. Lang, B. Anasori, D. Pinto, Y. Pivak, J. T. van Omme, S. J. May, Y. Gogotsi, M. L. Taheri, *Nat. Commun.* **2019**, *10*, 522.
[181] A. V. Mizrak, S. Uzun, B. Akuzum, L. Agartan, Y. Gogotsi, E. C. Kumbur, *J. Electrochem. Soc.* **2021**, *168*, 090518.
[182] A. Bhat, S. Anwer, K. S. Bhat, M. I. H. Mohideen, K. Liao, A. Qurashi, *npj 2D Materials and Applications* **2021**, *5*, 61.
[183] M. Ghidiu, M. R. Lukatskaya, M.-Q. Zhao, Y. Gogotsi, M. W. Barsoum, *Nature* **2014**, *516*, 78-81.
[184] P. Simon, *ACS Nano* **2017**, *11*, 2393-2396.
[185] H. Riazi, S. K. Nemani, M. C. Grady, B. Anasori, M. Soroush, *J. Mater. Chem. A* **2021**, *9*, 8051-8098.
[186] K. Maleski, V. N. Mochalin, Y. Gogotsi, *Chem. Mater.* **2017**, *29*, 1632-1640.
[187] Z. Lin, H. Shao, K. Xu, P.-L. Taberna, P. Simon, *Trends Chem.* **2020**, *2*, 654-664.
[188] F. Cao, Y. Zhang, H. Wang, K. Khan, A. K. Tareen, W. Qian, H. Zhang, H. Ågren, *Adv. Mater.* **2022**, *34*, 2107554.
[189] aM. Gyu Jung, G. Sambhaji Gund, Y. Gogotsi, H. Seok Park, *Batter. Supercaps* **2020**, *3*, 354-360; bJ. Orangi, M. Beidaghi, *Adv. Funct. Mater.* **2020**, *30*, 2005305.
[190] L. Wei, C. Xiong, H. Jiang, X. Fan, T. Zhao, *Energy Storage Mater.* **2020**, *25*, 885-892.
[191] E. Kohn, in *Comprehensive Microsystems* (Eds.: Y. B. Gianchandani, O. Tabata, H. Zappe), Elsevier, Oxford, **2008**, pp. 131-181.
[192] C. M. Van Genuchten, S. R. Bandaru, E. Surorova, S. E. Amrose, A. J. Gadgil, J. Pena, *Chemosphere* **2016**, *153*, 270-279.
[193] C.-H. Huang, L. Chen, C.-L. Yang, *Sep. Purif. Technol.* **2009**, *65*, 137-146.